

## Research paper

New heptacoordinate tungsten(II) complexes with  $\alpha$ -diimine ligands in the catalytic oxidation of multifunctional olefins

Maria Vasconcellos-Dias<sup>a</sup>, Carla D. Nunes<sup>a,b,\*</sup>, Vítor Félix<sup>c</sup>, Paula Brandão<sup>c</sup>,  
Maria José Calhorda<sup>a,d,\*</sup>

<sup>a</sup> Centro de Química e Bioquímica, Departamento de Química e Bioquímica, Faculdade de Ciências, Universidade de Lisboa, Campo Grande, 1749-016 Lisboa, Portugal

<sup>b</sup> Centro de Química Estrutural, Faculdade de Ciências, Universidade de Lisboa, 1049-001 Lisboa, Portugal

<sup>c</sup> CICECO - Aveiro Institute of Materials, Department of Chemistry, University of Aveiro, 3810-193 Aveiro, Portugal

<sup>d</sup> BioISI - Biosystems & Integrative Sciences Institute, Departamento de Química e Bioquímica, Faculdade de Ciências, Universidade de Lisboa, Campo Grande, 1749-016 Lisboa, Portugal

## ARTICLE INFO

Dedicated to Maurizio Peruzzini on the occasion of his 65th birthday

## Keywords:

Molybdenum

Tungsten

MCM-41

Catalysis

2-iminomethylpyridine

DFT calculations

## ABSTRACT

New tungsten(II) and molybdenum(II) heptacoordinate complexes  $[\text{MX}_2(\text{CO})_3(\text{L}_Y)]$  ( $\text{MXL}_Y$ : M = W, Mo; X = Br, I;  $\text{L}_Y = \text{C}_5\text{H}_4\text{NCY} = \text{N}(\text{CH}_2)_2\text{CH}_3$  with Y = H ( $\text{L}_1$ ), Me ( $\text{L}_2$ ), Ph ( $\text{L}_3$ )) were synthesized and characterized by spectroscopic techniques and elemental analysis. The two tungsten complexes  $\text{WXL}_1$  (X = Br, I) were also structurally characterized by single crystal X-ray diffraction. The metal coordination environment is in both a distorted capped octahedron. The complexes with  $\text{L}_1$  and  $\text{L}_2$  ligands were grafted in MCM-41, after functionalization of the ligands with a  $\text{Si}(\text{OEt})_3$  group. The new materials were characterized by elemental analysis,  $\text{N}_2$  adsorption isotherms,  $^{29}\text{Si}$  MAS and  $^{13}\text{C}$  MAS NMR. The tungsten(II) complexes and materials were the first examples of this type reported. All complexes and materials were tested as homogeneous and heterogeneous catalysts in the oxidation of multifunctional olefins (*cis*-hex-3-en-1-ol, *trans*-hex-3-en-1-ol, geraniol, S-limonene, and 1-octene), with *tert*-butyl hydroperoxide (TBHP) as oxidant. The molybdenum(II) catalyst precursors are in general very active, reaching 99% conversion and 100% selectivity in the epoxidation of *trans*-hex-3-en-1-ol. Their performance is comparable with that of the  $[\text{Mo}(\eta^3\text{-C}_3\text{H}_5)\text{X}(\text{CO})_2(\text{L}_Y)]$  complexes, but it increases with immobilization. On the other hand, most of the W(II) complexes display an activity similar or inferior to that of the Mo(II) analogues and it decreases after they are supported in MCM-41. DFT calculations show that tungsten complexes and iodide ligands are more easily oxidized from M(II) to M(VI) than molybdenum ones, while the energies of relevant species in the catalytic cycle are very similar for all complexes, making the theoretical rationalization of experimental catalytic data difficult.

## 1. Introduction

The number of tungsten complexes is in general much smaller than that of molybdenum complexes and usually it is not possible to compare the role of the metal in their applications, such as catalysis. Unlike Mo, W complexes with the very versatile bidentate  $\alpha$ -diimines ligands are few. These ligands give the metal a variety of environments and substituents for the two nitrogen atoms. In particular, in *N*-isopropyl 2-iminomethylpyridine (IMP, Scheme 1), the pyridyl and the imine confer to the ligand an asymmetry different from what substitution may cause in 2,2'-bipyridyl or 1,10-phenanthroline. Many molybdenum and some tungsten complexes of IMP have been described. The Mo(VI) complex  $[\text{MoO}_2\text{Cl}_2(\text{IMP})]$  was synthesized and immobilized in a micelle-

templated silica; both species were active in olefin epoxidation, but the activity was smaller in the material [1].  $[\text{Mo}(0)(\text{CO})_4(\text{R}_1, \text{R}_2\text{-IMP})]$  ( $\text{R}_1 = \text{H, Me, Ph, R}_2 = \text{COOH, SO}_3\text{Na}$ ; [2]  $\text{R}_1 = \text{R}_2 = \text{Me}$  [3]) complexes were obtained and some catalyzed the polymerization of methyl methacrylate (MMA) [2].  $[\text{Mo}(\text{CO})_4(\text{IMP})]$  was grafted in MCM-41 and the authors studied the activity of the complex and the material in olefin epoxidation in ionic liquids [4]. The Mo(0) complexes were also used to prepare  $[\text{Mo}(\text{II})(\eta^3\text{-C}_3\text{H}_5)\text{Cl}(\text{CO})_2(\text{R}_1, \text{R}_2\text{-IMP})]$  ( $\text{R}_1 = \text{Me, R}_2 = \text{Me, Ph, Ph-2-OMe}$  and  $\text{R}_1 = \text{Ph, R}_2 = \text{Me, Ph,}$ ) [5] by reaction with allyl halides, but the tungsten(0) analogues [6] did not react to yield the analogous allyl complexes [5]. However, the synthesis of W(IV) complexes  $[\text{WBr}_4(\text{R}_1, \text{R}_2\text{-IMP})]$  ( $\text{R}_1 = \text{H, R}_2 = \text{Me, Et, } ^n\text{Pr, } ^t\text{Bu}$ ) was reported, as well as their magnetic properties which were studied by  $^1\text{H}$  NMR [7].

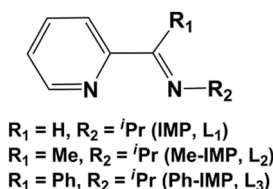
\* Corresponding authors.

<https://doi.org/10.1016/j.ica.2021.120263>

Received 25 October 2020; Received in revised form 15 January 2021; Accepted 15 January 2021

Available online 2 February 2021

0020-1693/© 2021 Elsevier B.V. All rights reserved.



Scheme 1. Representation of the IMP ligands.

Complexes of other metals containing IMP ligands have been used as catalysts and exhibited high activity. Some examples include Cu(I) for MMA polymerization [8], palladium nanoparticles immobilized in functionalized silica for the Suzuki-Miyaura cross coupling reaction and hydrogenation in water [9], or arene-Ru(II) complexes with functionalized chains ( $R_2$ ) for oxidative cleavage of 1-octene [10]. Complexes and clusters with IMP ligands often display interesting photochemical properties, as reported recently for  $[Os_3(CO)_{19}(IMP)]$  clusters [11]. We synthesized  $[Mo(\eta^3-C_3H_5)X(CO)_2(L)]$  ( $L = IMP$  ( $L_1$ ), Me-IMP ( $L_2$ ) and Ph-IMP ( $L_3$ ), Scheme 1) and prepared their heterogeneous counterparts by grafting them on MCM-41. For this system, immobilization did not always lead to improved efficiency [12].

Following our previous works on allylic Mo(II) complexes with IMP ligands, we report the synthesis of tungsten complexes  $[W(X)_2(CO)_3(IMP)]$  ( $L = IMP$  ( $L_1$ ),  $X = I, Br$ ). Moreover, given that Mo(II) analogues with  $L_1$  showed higher activity when acting as heterogeneous catalysts supported in MCM-41, than in homogeneous conditions, in the olefin epoxidation reaction [13], we also decided to prepare the  $M(X)_2(CO)_3$  complexes with the Me-IMP ( $L_2$ ) and Ph-IMP ( $L_3$ ) ligands ( $M = Mo$  and  $W$ ). All these complexes were further immobilized on MCM-41. The catalytic activity of these new complexes and materials was tested in the oxidation reactions of several olefins, some of them bearing the C=C bond and other functionalities.

Although oxidation catalysts are typically Mo(VI) complexes, it has been proved that  $[Mo(II)(\eta^5-C_5R_5)(CO)_3X]$  could be used as catalyst precursors to produce *in situ* the very active species  $[Mo(VI)(\eta^5-C_5R_5)O_2X]$  [14], which could be also isolated and characterized. Their activity could approach that of the highly active  $[Mo(\eta^3-C_3H_5)Cl(CO)_2(bian)]$  ( $bian$ ) 1,4-(4-chloro)phenyl-2,3-naphthalenediazabutadiene) was the first of another type of Mo(II) complexes, which, in the presence of TBHP, also originated catalysts almost as active as  $[Mo(VI)(\eta^5-C_5R_5)O_2X]$  [15]. Their main advantage was that the activity in the second run was as high as in the first. This was not observed in the  $Mo(VI)(\eta^5-C_5R_5)$  catalysts. Finally, some W(II) complexes behaved as oxidation catalysis precursors, as shown with the  $[MX_2(CO)_3(2-amino-1,3,4-thiadiazole)_2]$  ( $M = Mo, W$ ) complexes, which were synthesized and grafted in MCM-41. The W(II) precursors led to more active catalysts than Mo(II), and both became more active after immobilization in MCM-41 [16]. We want, in the present work, to explore the effect of having a bidentate  $\alpha$ -diimine instead of two

monodentate N-donor ligands.

## 2. Results and discussion

### 2.1. Chemical studies. Complexes

Tungsten and molybdenum complexes  $[MX_2(CO)_3(L_Y)]$  ( $MXL_Y$ :  $M = Mo, W$ ;  $X = Br, I$ ;  $L_Y = L_{1-3}$ ) were obtained by substitution of the nitriles in  $[MX_2(CO)_3(CH_3CN)_2]$  ( $X = Br, I$ ) by the ligands  $L_1$ ,  $L_2$ , and  $L_3$ , respectively, in dichloromethane during 4–6 h (Scheme 2). All the new complexes were characterized by elemental analysis, FTIR,  $^1H$  and  $^{13}C$  NMR spectroscopy, and complexes  $WBrL_2$  and  $WIL_2$  also by single crystal X-ray diffraction (*vide infra*). The two Mo(II) complexes with  $L_1$ ,  $MoBrL_1$  and  $MoIL_1$ , were previously reported [13]. The characterization will be more detailed for the new tungsten complexes of  $L_2$ .

In the FTIR spectra of both  $WBrL_2$  and  $WIL_2$  complexes in the solid state, the  $\nu C\equiv N$  vibrational modes of the precursor complexes have disappeared, while the  $\nu C=O$  stretching frequencies of the coordinated carbonyl groups were shifted from 1916 and 2028  $cm^{-1}$  to 1902, 1949 and 2033  $cm^{-1}$  in  $WBrL_2$ , and from 1889, 1906 and 1996  $cm^{-1}$  to 1925, 2003, 2019, and 2065  $cm^{-1}$  in  $WIL_2$  (Table S1). Three or four  $\nu C=O$  bands may be observed depending on the isomers present [17]. The  $\nu C=N$  stretching modes of the free ligand at 1655  $cm^{-1}$  were shifted to 1603 ( $WBrL_2$ ) and 1605  $cm^{-1}$  ( $WIL_2$ ) upon metal coordination. Similar trends were observed for the Mo(II) complexes (all values are collected in Table S1 of Supporting Information).

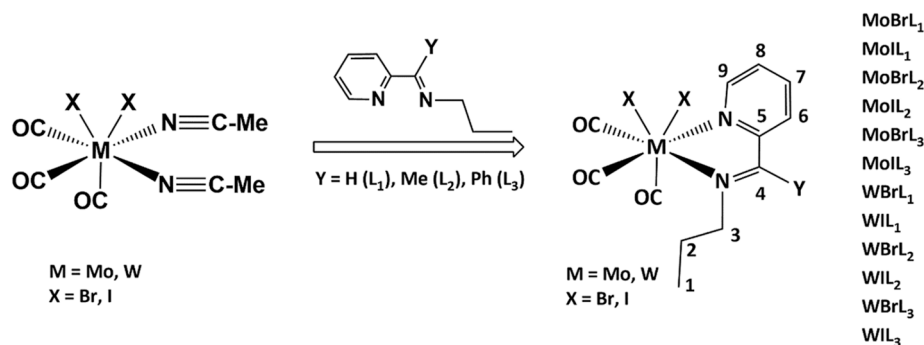
There is a tendency for the W complexes to have higher  $\nu C=O$  stretching frequencies than the Mo analogues, reflecting less back donation to the carbonyl ligands.

The  $^1H$  NMR spectra of complexes  $MoXL_2$ ,  $MoXL_3$ , and  $WXL_n$  ( $n = 1, 2, 3$ ;  $X = Br, I$ ) only show the peaks of the protons in the  $\alpha$ -diimine, which are shifted relatively to those of the free ligand. For example, in the tungsten complexes  $WBrL_2$  and  $WIL_2$ , the protons next to the donor nitrogen atoms,  $H_3$  and  $H_9$ , appear in the free ligand at 3.56 and 8.55 ppm, respectively, and are shifted to higher (downfield)  $\delta$  values at 3.84 ( $H_3$ ) and 8.76 ppm ( $H_9$ ) in  $WBrL_2$  and 3.78 ( $H_3$ ) and 9.56 ppm ( $H_9$ ) in  $WIL_2$ . The other three aromatic protons  $H_6$ ,  $H_7$  and  $H_8$  are shifted from 8.03 to 8.40 ppm ( $H_6$ ), 7.21 to 8.52 ppm ( $H_7$ ), and 7.64 to 7.82 ppm ( $H_8$ ) in complex  $WIL_2$ . The assignments were made with resort to bidimensional COSY and HMQC experiments.

The  $^{13}C$  NMR spectra of  $WBrL_2$  and  $WIL_2$  exhibit peaks assigned to the  $C_3$  and  $C_9$  carbons at 54.2 and 149.1 ppm, and at 44.0 and 151.0 ppm, respectively.  $C_9$  experiences the largest shift relative to the free ligand  $L_2$ . These and other peaks arising from the other carbon atoms are also observed for all the complexes (Experimental).

The molecular structures of complexes  $WBrL_1$  and  $WIL_1$  were determined by single crystal X-ray diffraction analysis and are shown in Figs. 1 and 2, respectively.

These two complexes have a coordination number 7, for which three main alternative structures are possible, namely pentagonal bipyramid,



Scheme 2. The synthesis of molybdenum(II) and tungsten(II)  $[MX_2(CO)_3(L_Y)]$  ( $MXL_Y$ ) complexes and the numbering scheme for NMR of carbons and respective hydrogens.

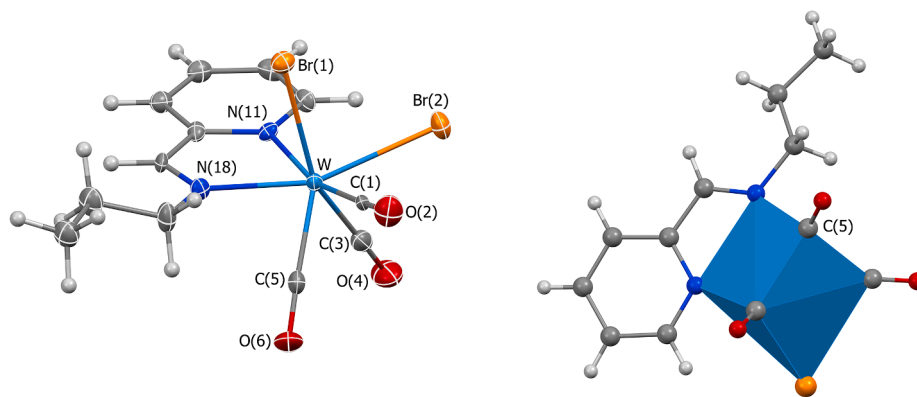


**Fig. 1.** Molecular structure of  $[\text{WBr}_2(\text{CO})_3(\text{L}_1)]$  ( $\text{WBrL}_1$ ) in two different views: thermal ellipsoids (50% probability level) showing the overall structure (left); capped octahedral tungsten coordination geometry (right).

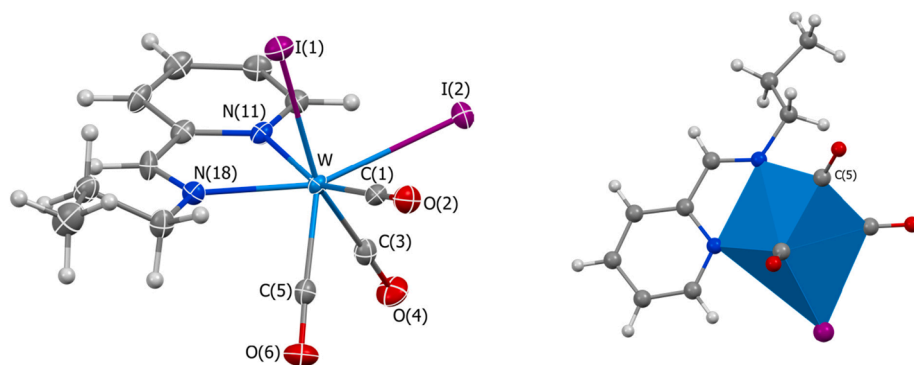
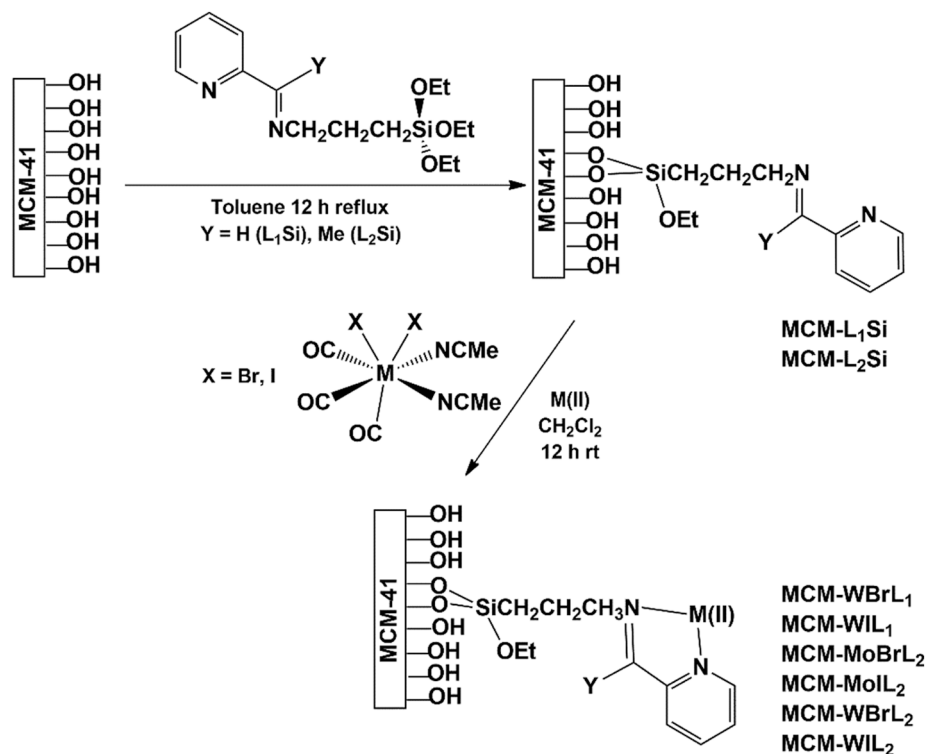


**Fig. 2.** Molecular structure of  $[\text{WBr}_2(\text{CO})_3(\text{L}_1)]$  ( $\text{WIL}_1$ ) in two different views: thermal ellipsoids (50% probability level) showing the overall structure (left); capped octahedral tungsten coordination geometry (right).



**Scheme 3.** Procedure for the immobilization of complexes  $\text{MoXL}_2$ ,  $\text{WXL}_1$  and  $\text{WXL}_2$  (X = Br, I) in MCM.

capped trigonal prism, and capped octahedron. The coordination geometries of **WBrL<sub>1</sub>** and **WIL<sub>1</sub>** can be described as a distorted capped octahedron. The carbonyl ligand C(5) is capping the triangular face C(3)–N(18)–C(1), with bond angles C(5)–W–C(3), C(5)–W–N(18) and C(5)–W–C(1) ranging from 71.7(2) to 75.9(2)° for **WBrL<sub>1</sub>** and from 71.8(2) to 77.8(2) for **WIL<sub>1</sub>**. This face is opposite to the X(1)–N(11)–X(2) one (X = Br, **WBrL<sub>1</sub>** and X = I, **WIL<sub>1</sub>**, Figs. 1 and 2 right). Moreover, the chelation of the bidentate ligand IMP, through the two nitrogen donors, one halide (X(2) with X = I or Br) and one carbonyl ligand C(1), occurs in the equatorial plane of the metal coordination sphere (Figs. 1 and 2 left). In the molecular structure of **WBrL<sub>1</sub>**, the W–N(11) and W–N(18) distances are 2.217(4) and 2.172(4) Å, respectively and in **WIL<sub>1</sub>** the same atom distances are 2.216(4) and 2.180(4) Å, respectively. These distances lead to N(11)–W–N(18) bite angles, for the five membered chelate ring, of 72.9 (2) and 72.7(1)° for **WBrL<sub>1</sub>** and **WIL<sub>1</sub>**, respectively. Bond lengths and bond angles around the tungsten center are given in Table S2 (SI) for both complexes.

## 2.2. Chemical studies. Materials

The new complexes **WXL<sub>1</sub>** and **WXL<sub>2</sub>** (X = Br, I) and **MoXL<sub>2</sub>** were immobilized in MCM-41 (**MCM**) according to the procedure reported for **MoXL<sub>1</sub>** (X = Br, I) and described in Scheme 3 for the new compounds [12]. MCM-41 (**MCM**) was synthesized by a template approach [18].

The silylated ligands **L<sub>1</sub>Si** and **L<sub>2</sub>Si** reacted with the **MCM** surface OH groups to afford the ligand functionalized materials **MCM–L<sub>1</sub>Si** and **MCM–L<sub>2</sub>Si**. Then, the reaction between these materials and the precursor complexes [MX<sub>2</sub>(CO)<sub>3</sub>(CH<sub>3</sub>CN)<sub>2</sub>] (M = W, Mo; X = Br, I) led to the formation of new containing materials of W and Mo: **MCM–WBrL<sub>1</sub>**, **MCM–WIL<sub>1</sub>**, **MCM–WBrL<sub>2</sub>**, **MCM–WIL<sub>2</sub>**, **MCM–MoBrL<sub>2</sub>**, and **MCM–MoIL<sub>2</sub>**, which are similar to **MCM–MoXL<sub>1</sub>** (X = Br, I) described previously [12]. For the tungsten materials **MCM–WBrL<sub>2</sub>** and **MCM–WIL<sub>2</sub>**, the metal content was found by elemental analysis to be 3.4 wt% (0.19 mmol g<sup>−1</sup>) and 4.47 wt% (0.26 mmol g<sup>−1</sup>). Mo loads of 5.11 wt% (0.53 mmol g<sup>−1</sup>) and 5.97 wt% (0.62 mmol g<sup>−1</sup>) were determined for **MCM–MoBrL<sub>2</sub>** and **MCM–MoIL<sub>2</sub>**, respectively.

It is possible to conclude that all the metal fragments reacted with the ligand **L<sub>2</sub>** at the surface of the material, as the load of ligand was much higher. Indeed, based on the nitrogen analysis for each material, loads of the **L<sub>2</sub>** ligand of 0.80 and 0.39 mmol g<sup>−1</sup>, for **MCM–WBrL<sub>2</sub>** and **MCM–WIL<sub>2</sub>**, and 0.77 and 0.82 mmol g<sup>−1</sup>, for **MCM–MoBrL<sub>2</sub>** and **MCM–MoIL<sub>2</sub>**, were found.

All materials were also characterized by powder XRD, DRIFT, and <sup>29</sup>Si MAS and <sup>13</sup>C CP MAS NMR. Sorption/desorption N<sub>2</sub> isotherms were also determined for estimation of textural parameters. All characterization features are consistent with those reported in related mesoporous materials [12,13,18].

The X-ray diffraction powder patterns of the initial **MCM** (Figure S1, SI) show peaks in the 2θ range between 2 and 10°, which can be indexed to the (100), (110), (200) and (210) reflections. They display a diffraction pattern with a hexagonal symmetry revealing the existence of a periodic arrangement of hexagonal channels in the materials. From the *d*<sub>100</sub> interplanar value of the 100 reflection (35.7 Å), the lattice constant *a* = 2*d*<sub>100</sub>/√3 is estimated as 41.2 Å.

After functionalization of **MCM** with the silylated ligand **L<sub>2</sub>Si**, the new **MCM–L<sub>2</sub>Si** material still shows the three peaks corresponding to three reflections, but they are shifted slightly towards higher 2θ values as compared with **MCM-41**. The *d* distance for the 100 reflection increases to 36.2 Å, corresponding to a constant lattice of *a* = 41.8 Å. The same periodic hexagonal arrangement was also found for materials **MCM–MoBrL<sub>2</sub>**, **MCM–MoIL<sub>2</sub>**, **MCM–WBrL<sub>2</sub>** and **MCM–WIL<sub>2</sub>**, obtained from **L<sub>2</sub>Si** by reaction with the metal precursors. Their *d*<sub>100</sub> distances of 35.9 Å, 36.4 Å, 36.0 Å, and 35.9 Å correspond to lattice constants *a* = 41.5 Å, 42.0 Å, 41.6 Å, and 41.5 Å, respectively, as collected in Table 1. Similar results were observed for the tungsten materials **MCM–WBrL<sub>1</sub>**

**Table 1**

Textural parameters of host and composite materials from powder XRD and N<sub>2</sub> isotherms at 77 K, for **MCM**, **MCM–L<sub>2</sub>**, **MCM–MoBrL<sub>2</sub>**, **MCM–MoIL<sub>2</sub>**, **MCM–WBrL<sub>2</sub>**, and **MCM–WIL<sub>2</sub>** materials.

Sample	<i>d</i> <sub>100</sub> (Å)	<i>S</i> <sub>BET</sub> m <sup>2</sup> . g <sup>−1</sup>	Δ <i>S</i> <sub>BET</sub> (%)	<i>V</i> <sub>p</sub> cm <sup>3</sup> . g <sup>−1</sup>	Δ <i>V</i> <sub>p</sub> <sup>b</sup> (%)	<i>d</i> <sub>BJH</sub> (nm)
<b>MCM</b>	35.7	1037	–	0.97	–	3.60
<b>MCM–L<sub>2</sub></b>	36.2	674	35.0	0.42	56.7	2.87
<b>MCM–MoBrL<sub>2</sub></b>	35.9	628	39.4	0.39	59.8	2.67
<b>MCM–MoIL<sub>2</sub></b>	36.4	609	41.3	0.44	54.6	2.86
<b>MCM–WBrL<sub>2</sub></b>	36.0	578	44.3	0.39	59.8	2.86
<b>MCM–WIL<sub>2</sub></b>	35.9	458	55.8	0.27	72.2	2.65

and **MCM–WIL<sub>1</sub>** and were previously reported for **MCM–MoBrL<sub>1</sub>** and **MCM–MoIL<sub>1</sub>** [13].

The intensity of the peaks is reduced as the stepwise functionalization takes place, but it is more significant in the materials with the Mo and W cores. This effect does not derive from a decreased crystallinity of the materials, but to a reduction of the X-ray scattering contrast between the **MCM** silica walls and the metal complexes inside the pores, as has been demonstrated before [19,20].

Nitrogen sorption/desorption studies, performed at 77 K, revealed for all the materials a reversible type IV isotherm (Fig. 3), typical of mesoporous MCM-41 materials (pore width between 2 nm and 50 nm, according to IUPAC) [21]. The textural parameters *S*<sub>BET</sub> and *V*<sub>p</sub> were calculated for all materials (Table 1) and showed values comparable with those in literature data [22]. The capillary condensation/evaporation step is observed in all the materials between 0.33 and 0.42 relative pressures, and they have a uniform pore size distribution as reflected in the sharpness of the step.

*S*<sub>BET</sub> and *V*<sub>p</sub> calculated for **MCM–L<sub>2</sub>** display a decrease relative to **MCM** of 35% and 57%, respectively, in accordance with the decrease in *p/p*<sub>0</sub> coordinates of the inflection points of the isotherms [23]. The size of the capillary condensation step, which is related to the volume of pore space spanned by the pore walls, becomes even smaller for the modified materials **MCM–MoBrL<sub>2</sub>**, **MCM–MoIL<sub>2</sub>**, **MCM–WBrL<sub>2</sub>** and **MCM–WIL<sub>2</sub>**. The maximum of the pore size distribution (PSD) curve (Fig. 3), determined by the BJH method (*d*<sub>BJH</sub>), drops from 3.60 to 2.87 nm when going from **MCM** to **MCM–L<sub>2</sub>**. When the metal fragments are introduced in **MCM–L<sub>2</sub>**, they produce a relative decrease in *S*<sub>BET</sub> which amounts to 44%, 56%, 39% and 41%, for **MCM–WBrL<sub>2</sub>**, **MCM–WIL<sub>2</sub>**, **MCM–MoBrL<sub>2</sub>** and **MCM–MoIL<sub>2</sub>**, respectively, when compared to **MCM**. The values of *V*<sub>p</sub> for materials **MCM–WBrL<sub>2</sub>**, **MCM–WIL<sub>2</sub>**, **MCM–MoBrL<sub>2</sub>** and **MCM–MoIL<sub>2</sub>**, also reveal a more pronounced decrease of 60%, 72%, 60% and 55%, respectively.

The distribution of pore size, obtained by the BJH method, decreases after the functionalization step. The size of the pore starts at 3.6 nm for the parent **MCM**, dropping to 2.87 nm after the introduction of the **L<sub>2</sub>Si** ligand, and continues to decrease to 2.67, 2.86, 2.86 and 2.65 nm, respectively, for materials **MCM–MoBrL<sub>2</sub>**, **MCM–MoIL<sub>2</sub>**, **MCM–WBrL<sub>2</sub>** and **MCM–WIL<sub>2</sub>**. This trend in the pore size shows that the ligand and the metal fragments have functionalized the walls inside the pores.

The DRIFT spectrum of the **MCM** host (Figure S2) evidences a broad band in the 3600–2600 cm<sup>−1</sup> range, typical of silicates, assigned to hydrogen bonded silanol groups. The band at ca. 1600 cm<sup>−1</sup> due to OH bending modes and the intense broad band at 1230–900 cm<sup>−1</sup> assigned to the asymmetric stretching vibration modes of the mesoporous framework (νSi–O–Si) are other relevant features. In **MCM–L<sub>2</sub>** containing the grafted organic ligand **L<sub>2</sub>Si**, several changes and new bands are detected. The most remarkable feature is the new band at 1640 cm<sup>−1</sup> corresponding to the C=N stretching vibrations from the imine part of the ligand **L<sub>2</sub>Si**.

The introduction of the M(CO)<sub>3</sub>X<sub>2</sub> fragments to yield **MCM–MoBrL<sub>2</sub>**, **MCM–MoIL<sub>2</sub>**, **MCM–WBrL<sub>2</sub>** and **MCM–WIL<sub>2</sub>** also modifies the spectral features, owing to the three new bands assigned to the νC≡O (Figure S2) modes. These bands, slightly shifted relatively to those of the precursor



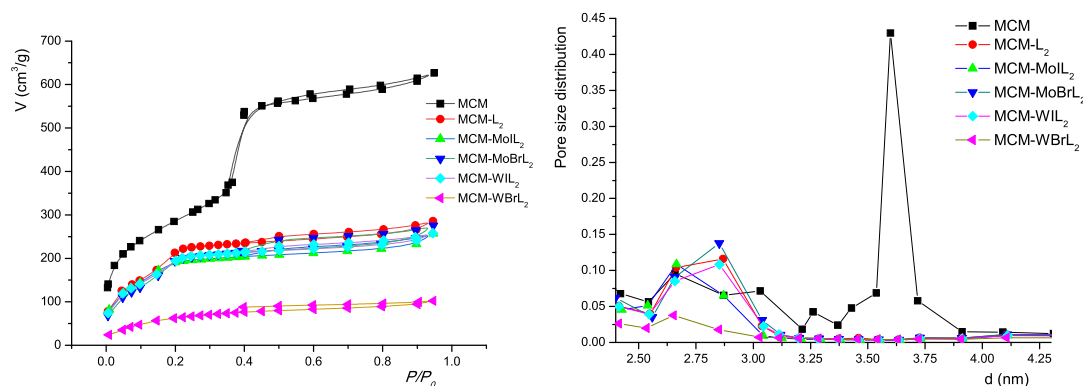


Fig. 3. Nitrogen adsorption studies of MCM and functionalized materials MCM-L<sub>2</sub>, MCM-MoBrL<sub>2</sub>, MCM-MoIL<sub>2</sub>, MCM-WBrL<sub>2</sub> and MCM-WIL<sub>2</sub> at 77 K: isotherms (left) and pore size distribution curves (right).

complexes, are observed for MCM-WBrL<sub>2</sub> at 1632, 1555 and 1865 cm<sup>-1</sup>. The νC=N stretching vibrations of MCM-WBrL<sub>2</sub> are detected at 1632 and 1591 cm<sup>-1</sup> (Fig. 5), showing the integrity of the ligand and its coordination to the core. The values are similar for the other materials.

All materials were also characterized by <sup>13</sup>C and <sup>29</sup>Si MAS solid-state NMR (Fig. 4). The <sup>29</sup>Si MAS NMR spectrum of pristine MCM displays two broad resonances at -109.3 and -100.4 ppm, assigned to Q<sup>4</sup> and Q<sup>3</sup> species, and a weak shoulder at -92.1 ppm assigned to Q<sup>2</sup> species. Q<sup>n</sup> species arise from the silica framework [Q<sup>n</sup> = Si(OSi)<sub>n</sub>(OH)<sub>4-n</sub>], the Q<sup>3</sup> sites being associated with single silanols Si-OH, often involved in hydrogen bonding, and the Q<sup>2</sup> sites with Si-(OH)<sub>2</sub> groups (Fig. 4). MCM-L<sub>2</sub> shows signals at -109.6, -101.2 and -91.7 ppm for the Q<sup>4</sup>, Q<sup>3</sup> and Q<sup>2</sup> species, respectively, shifted from those of the MCM precursor. The L<sub>2</sub>Si ligand present in MCM-L<sub>2</sub> has a different silicon atom, responsible for the signals associated to T<sup>n</sup> species. Resonances at -66.4, -57.5 and -47.9 ppm assigned to the T<sup>3</sup>, T<sup>2</sup> and T<sup>1</sup> species are thus also observed. The Q<sup>n</sup> and T<sup>n</sup> species resonances are observed in all the derivatized materials and reflect the immobilization of the ligands and complexes in the MCM.

The <sup>29</sup>Si MAS spectra of MCM-MoBrL<sub>2</sub>, MCM-MoIL<sub>2</sub>, MCM-WBrL<sub>2</sub> and MCM-WIL<sub>2</sub> do not differ significantly from that of MCM-L<sub>2</sub>, indicating that the reaction of the precursors MX<sub>2</sub>(MeCN)<sub>2</sub>(CO)<sub>3</sub> (M = Mo or W; X = Br or I) occurs with the nitrogen donor atoms in MCM-L<sub>2</sub> material and not with the material walls, as in this case the Si signals Q<sup>n</sup> from the surface and T<sup>n</sup> from the ligands would change more. For MCM-

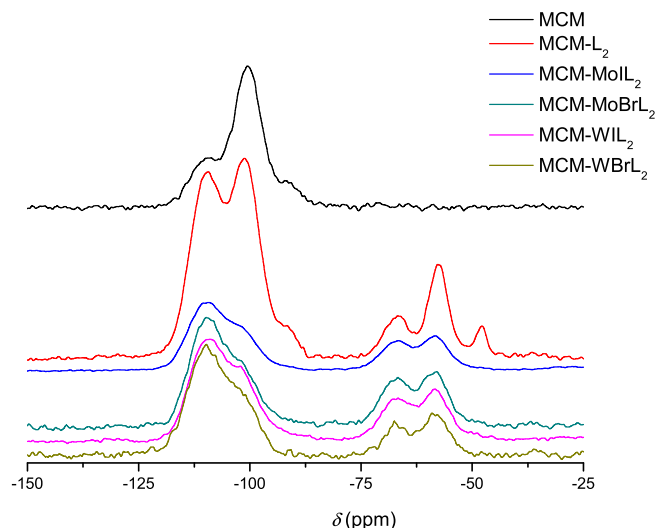


Fig. 4. <sup>29</sup>Si MAS NMR spectra of the MCM parent and corresponding functionalized materials MCM-L<sub>2</sub>, MCM-MoBrL<sub>2</sub>, MCM-MoIL<sub>2</sub>, MCM-WBrL<sub>2</sub> and MCM-WIL<sub>2</sub>.

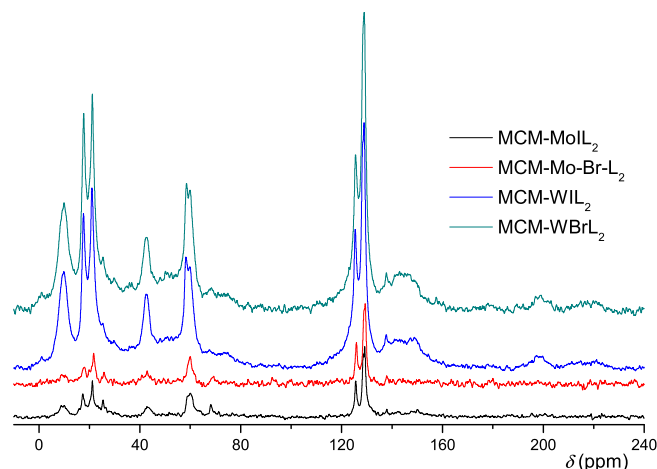


Fig. 5. <sup>13</sup>C CP MAS NMR spectra of MCM functionalized materials MCM-L<sub>2</sub>, MCM-MoBrL<sub>2</sub>, MCM-MoIL<sub>2</sub>, MCM-WBrL<sub>2</sub> and MCM-WIL<sub>2</sub>.

WBrL<sub>2</sub> the resonances appear at -109.8 (Q<sup>4</sup>) and -102.4 (Q<sup>3</sup>) ppm, and at -67.6 (T<sup>3</sup>) and -59.0 (T<sup>2</sup>) ppm.

The <sup>13</sup>C CP MAS NMR spectrum (not shown) of material MCM-L<sub>2</sub> is very similar to that of the L<sub>2</sub> ligand, suggesting that the ligand is bound to the surface of material and was not affected by the immobilization procedure. It shows two broad signals corresponding to the aromatic carbons of the pyridine ring at 123.2 and 127.5 ppm. The protons of the alkyl chain of the ligand (1, 2, 3 in Scheme 2) show signals at 9.5, 21.0, and 43.0 ppm, which were assigned to SiCH<sub>2</sub>CH<sub>2</sub>CH<sub>2</sub>N, SiCH<sub>2</sub>CH<sub>2</sub>CH<sub>2</sub>N and SiCH<sub>2</sub>CH<sub>2</sub>CH<sub>2</sub>N. The <sup>13</sup>C NMR spectra of the metal containing materials MCM-MoBrL<sub>2</sub>, MCM-MoIL<sub>2</sub>, MCM-WBrL<sub>2</sub> and MCM-WIL<sub>2</sub> (Fig. 5) are not very different, suggesting that the presence of the Mo nuclei practically does not modify the chemical environment experienced by the carbon nuclei of the ligand. The spectra display signals at around 9.0–10.0 ppm assigned to the SiCH<sub>2</sub>CH<sub>2</sub>CH<sub>2</sub>N atom, at around 22 ppm to SiCH<sub>2</sub>CH<sub>2</sub>CH<sub>2</sub>N, and at around 43 ppm corresponding to the carbon adjacent to the nitrogen atom, SiCH<sub>2</sub>CH<sub>2</sub>CH<sub>2</sub>N. The Si atom is still bound to one OEt group (Scheme 3), with signals at 18 and 59.5 ppm, belonging to CH<sub>3</sub> and CH<sub>2</sub>, respectively. The carbon atom 4 (Scheme 2) is observed at 67 ppm and the CH<sub>3</sub> (Y substituent, Scheme 2) at ~ 60 ppm.

### 2.3. Catalytic studies. Complexes

All complexes, WXL<sub>n</sub> (L<sub>n</sub> = L<sub>1</sub>, L<sub>2</sub>, L<sub>3</sub>; X = Br, I), and MoXL<sub>2</sub> (X = Br, I), MoXL<sub>3</sub> (X = Br, I), were tested as catalyst precursors in the epoxidation catalysis of the set of multifunctional olefins *cis*-hex-3-en-1-ol

(cis), *trans*-hex-3-en-1-ol (trans), geraniol (ger), *S*-limonene (lim) and 1-octene (1-oct), with *tert*-butyl hydroperoxide (TBHP) as oxygen donor, using dichloromethane as solvent, at 328 K. The results obtained are summarized in Table 2 (see details in Experimental section). No reaction occurs in the absence of a catalyst.

With very few exceptions, the complexes containing the iodide ligand were more active and selective than the complexes with the bromide ligand.

All the tested catalysts oxidized *cis*-hex-3-en-1-ol with 100% selectivity to the respective epoxide (entries 1–10). In general, those containing iodide show higher conversions than those with bromide. Tungsten complexes containing the ligand L<sub>1</sub>, WXL<sub>1</sub> (X = I, Br), and molybdenum complexes MoXL<sub>2</sub> (X = I, Br) showed fair to lower

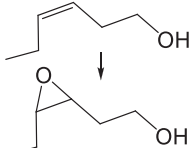
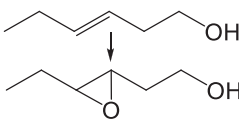
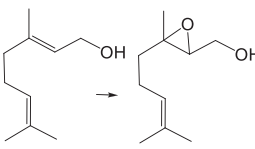
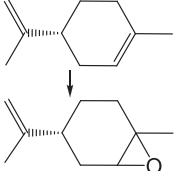
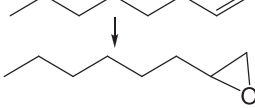
conversions, the tungsten catalysts being the ones with lowest conversion. However, catalysts MoXL<sub>3</sub>, WXL<sub>2</sub>, and WXL<sub>3</sub> (X = I, Br) showed very high conversions above 92%.

The epoxidation of *trans*-hex-3-en-1-ol is promoted by all catalysts with good substrate conversion (61–99%, Table 2, entries 11–20). Epoxidation of the *trans*-hex-3-en-1-ol olefin led to the formation of hexan-1-ol-3,4-epoxide (100%) in all cases, except with MoBrL<sub>2</sub> and WXL<sub>1</sub> (X = I, Br), which present high conversions (67, 90, and 89%) but a low or very low selectivity toward hexan-1-ol-3,4-epoxide (30, 20, and 10%).

The two non-equivalent C=C bonds of *S*-limonene and geraniol may give rise to two different epoxides upon oxidation. Those favored by the catalysts are sketched in Table 2 and correspond to epoxidation in the

**Table 2**

Olefin epoxidation catalyzed with complexes MXL<sub>y</sub> (M = Mo, W, L<sub>n</sub> = L<sub>1</sub>, L<sub>2</sub>, L<sub>3</sub> X = Br, I) of *cis*-hex-3-en-1-ol (*cis*), *trans*-hex-3-en-1-ol (*trans*), geraniol (ger), *S*-limonene and 1-octene (oct).

Entry	Substrate <sup>a</sup>	Catalyst	Conv. <sup>b</sup> %	Select. <sup>c</sup> %	Yield %
1	 <i>cis</i> -hex-3-en-1-ol	WBrL <sub>1</sub>	3	100	3
2		WIL <sub>1</sub>	14	100	14
3		WBrL <sub>2</sub>	97	100	97
4		WIL <sub>2</sub>	100	100	100
5		WBrL <sub>3</sub>	99	100	99
6		WIL <sub>3</sub>	92	100	92
7		MoBrL <sub>2</sub>	18	100	18
8		MoIL <sub>2</sub>	41	100	41
9		MoBrL <sub>3</sub>	95	100	95
10		MoIL <sub>3</sub>	98	100	98
11	 <i>trans</i> -hex-3-en-1-ol	WBrL <sub>1</sub>	89	10	9
12		WIL <sub>1</sub>	90	22	20
13		WBrL <sub>2</sub>	61	100	61
14		WIL <sub>2</sub>	96	100	96
15		WBrL <sub>3</sub>	75	100	75
16		WIL <sub>3</sub>	82	100	82
17		MoBrL <sub>2</sub>	67	30	20
18		MoIL <sub>2</sub>	67	100	67
19		MoBrL <sub>3</sub>	99	100	99
20		MoIL <sub>3</sub>	89	100	89
21	 Geraniol	WBrL <sub>1</sub>	89	82	73 <sup>d</sup>
22		WIL <sub>1</sub>	86	80	59/10 <sup>d</sup>
23		WBrL <sub>2</sub>	100	60	60 <sup>d</sup>
24		WIL <sub>2</sub>	100	86	43/43 <sup>d</sup>
25		WBrL <sub>3</sub>	85	82	45/25 <sup>d</sup>
26		WIL <sub>3</sub>	92	92	46/46 <sup>d</sup>
27		MoBrL <sub>2</sub>	100	77	61/6 <sup>d</sup>
28		MoIL <sub>2</sub>	100	86	80/2 <sup>d</sup>
29		MoBrL <sub>3</sub>	97	100	97 <sup>d</sup>
30		MoIL <sub>3</sub>	98	100	89/9 <sup>d</sup>
31	 <i>S</i> -limonene	WBrL <sub>1</sub>	5	62	3/0/0 <sup>e</sup>
32		WIL <sub>1</sub>	24	76	9/9/0 <sup>e</sup>
33		WBrL <sub>2</sub>	100	8	8/0/78 <sup>e</sup>
34		WIL <sub>2</sub>	100	4	2/2/96 <sup>e</sup>
35		WBrL <sub>3</sub>	97	26	12/14/76 <sup>e</sup>
36		WIL <sub>3</sub>	31	18	2/4/19 <sup>e</sup>
37		MoBrL <sub>2</sub>	100	78	64/14/0 <sup>e</sup>
38		MoIL <sub>2</sub>	100	83	57/26/0 <sup>e</sup>
39		MoBrL <sub>3</sub>	100	9	5/4/90 <sup>e</sup>
40		MoIL <sub>3</sub>	100	20	8/12/80 <sup>e</sup>
41	 1-octene	WBrL <sub>1</sub>	42	27	2
42		WIL <sub>1</sub>	2	100	1
43		WBrL <sub>2</sub>	30	94	26
44		WIL <sub>2</sub>	34	91	31
45		WBrL <sub>3</sub>	5	77	4
46		WIL <sub>3</sub>	39	93	36
47		MoBrL <sub>2</sub>	1	100	1
48		MoIL <sub>2</sub>	9	67	6
49		MoBrL <sub>3</sub>	33	96	31
50		MoIL <sub>3</sub>	68	94	64

<sup>a</sup> All reactions were carried out in dichloromethane in the presence of 2 eq. of oxidant (TBHP) and 1 mol % of M catalyst (M = Mo or W) at 328 K, preferred epoxide shown; <sup>b</sup> Calculated after 24 h; <sup>c</sup> Calculated as "Yield of epoxide"/"Conversion"\*100%; <sup>d</sup> Yield of 2,3-/6,7-oxirane epoxides; <sup>e</sup> Yield of Z-epoxide, E-epoxide, and di-epoxide.

2,3 positions, for geraniol, and in the ring, for *S*-limonene.

All complexes led to very high conversion (85–100%) of geraniol with high selectivity (60–100%). The 2,3-oxirane epoxide (Table 2) was preferred, but variable amounts of the 6,7-oxirane epoxide were also obtained. The tungsten complexes **WIL**<sub>2</sub> and **WIL**<sub>3</sub> showed similar selectivity for the two epoxides (43/43 and 46/46% for 2,3-/6,7-oxirane epoxides, respectively), and **WBrL**<sub>3</sub> behaved similarly with a 45/25% ratio (entries 24–26). The highest conversion and selectivity toward the 2,3-oxirane epoxide was obtained with **MoBrL**<sub>3</sub> (97%, entry 29). **WBrL**<sub>1</sub> and the **WIL**<sub>2</sub> had 100% conversions, but selectivity was lower (entries 23 and 24). The remaining catalysts showed a preference for the 2,3 product, but the 6,7 was also formed.

When the substrate is *S*-limonene (Table 2, entries 31–40), conversions of 100% are reached with the molybdenum catalysts and **WXL**<sub>2</sub>, **WXL**<sub>1</sub> are almost inactive (5 and 24%, for X = Br and I, respectively), while **WXL**<sub>3</sub> present 97 and 31% conversions, for X = Br and I. The *Z*- and *E*-epoxides are always observed, except with complexes **WBrL**<sub>1</sub> and **WBrL**<sub>2</sub> (only the *E*-epoxide), and the yield is never very good. The highest one for the *Z*-epoxide is 64% with **MoBrL**<sub>2</sub> (entry 37), and the values for the *E*-epoxide are much lower. High yield is observed for the double epoxide with catalysts **MoBrL**<sub>3</sub> (90%), **MoIL**<sub>3</sub> (80%), **WBrL**<sub>2</sub> (78%), **WIL**<sub>2</sub> (96%), and **WBrL**<sub>3</sub> (76%), in entries 39, 40, and 33–35.

The oxidation of 1-octene (Table 2, entries 41–50), an unbranched (not activated) terminal olefin, was achieved with medium to fair conversions by all complexes, reaching 68% with **MoIL**<sub>3</sub>. The highest yield of the epoxide was observed with the complexes **WBrL**<sub>2</sub>, **WIL**<sub>2</sub>, **WIL**<sub>3</sub>, **MoBrL**<sub>3</sub>, and **MoIL**<sub>3</sub>, catalyst (entries 43, 44, 46, 49, and 50), with yields from 26 to 64%.

We can compare the activity of the previous catalysts, especially those containing molybdenum, with that of the complexes [Mo( $\eta^3$ -C<sub>3</sub>H<sub>5</sub>)X(CO)<sub>2</sub>(L<sub>Y</sub>)] (L<sub>Y</sub> = L<sub>1</sub>, L<sub>2</sub>, and L<sub>3</sub>, respectively **1**, **2**, and **3**) [13]. These three complexes oxidized the *cis* substrate with 99% conversion and 100% selectivity, which is much better than that obtained with **MoBrL**<sub>2</sub> and **WBrL**<sub>1</sub>, slightly better than with **MoBrL**<sub>3</sub> and **WBrL**<sub>2</sub>, and the same as **WBrL**<sub>3</sub>. Complex **2** was more selective than **MoBrL**<sub>2</sub> for the epoxidation of *trans*, but **MoIL**<sub>3</sub>, on the other hand, converted *trans* with much higher selectivity and conversion than complex **3**. The conversions in the oxidation of *ger* catalyzed by complexes **1**, **2**, **3** and **MoXL**<sub>2,3</sub> (X = Br, I) were very similar. However, the four molybdenum complexes **MoXL**<sub>2,3</sub> (X = Br, I) were much more selective than **1**, **2**, and **3**, with high yields of the 2,3-oxirane product, while complexes **1–3** led to similar amounts of 2,3- and 6,7-oxirane. None of the two groups of complexes exhibited high conversions for the epoxidation of 1-octene, and selectivity was similar. **MoBrL**<sub>1</sub> and **MoIL**<sub>1</sub> were tested in a different group of substrates and cannot be easily compared. In general, no clear effect of the substitution pattern in L<sub>1</sub>, L<sub>2</sub> and L<sub>3</sub> is observed.

There are not extremely large differences between the W and the Mo catalysts. However, when the complexes [MX<sub>2</sub>(CO)<sub>3</sub>(2-amino-1,3,4-thiadiazole)<sub>2</sub>] (M = Mo, W) were tested, the W(II) ones were distinctly more active from those of Mo(II) [16]. We can compare the activity of these complexes with those in the present work in the oxidation of the common substrate *S*-limonene. The Mo(II) 2-amino-1,3,4-thiadiazole complexes have 0% conversion and MoX<sub>2</sub>L<sub>2</sub>/L<sub>3</sub> (X = Br, I) 100%, while the differences for W are small. This can be explained by the stronger W-L bonds, suggesting that the binuclear W(II) active species with the monodentate species is robust enough to undergo catalysis, while the Mo(II) is not. The chelation effect introduced by the  $\alpha$ -diimine ligands stabilizes the active species, making the Mo(II) catalysts more stable.

On the other hand, a comparative study of MCl<sub>2</sub>(O<sub>2</sub>) (M = Mo, W) derivatives showed that the performance of W catalysts in *cis*-cyclooctene epoxidation was higher in the presence of H<sub>2</sub>O<sub>2</sub> as oxidant, and lower when TBHP was used, emphasizing the subtle balance [24].

#### 2.4. Catalytic studies. Materials

All materials **MCM-WBrL**<sub>1</sub>, **MCM-WIL**<sub>1</sub>, **MCM-MoBrL**<sub>2</sub>, **MCM-MoIL**<sub>2</sub>, **MCM-WBrL**<sub>2</sub> and **MCM-WIL**<sub>2</sub> were tested as catalyst precursors for olefin epoxidation using the same multifunctional olefins as above: *cis*-hex-3-en-1-ol (*cis*), *trans*-hex-3-en-1-ol (*trans*), geraniol (*ger*), *S*-limonene (*lim*) and 1-octene (*oct*), using *tert*-butylhydroperoxide (TBHP in decane) as oxygen donor, in dichloromethane, at 328 K (see details in Experimental section). No reaction occurred in the absence of a catalyst.

All the tested catalysts are 100% selective towards the epoxide in the oxidation of *cis*-hex-3-en-1-ol (*cis*), as seen in Table 3, entries 1–6. While the molybdenum containing materials lead to 100% yield for the desired epoxide, the tungsten catalysts display modest conversions in the range 21–47%, the lowest being obtained with the Br containing materials. **MCM-MoBrL**<sub>2</sub> and **MCM-MoIL**<sub>2</sub>, as well as **MCM-WBrL**<sub>1</sub> and **MCM-WIL**<sub>1</sub>, are more active catalysts than the complexes, while **MCM-WBrL**<sub>2</sub> and **MCM-WIL**<sub>2</sub> become less active.

The same trends are observed for all catalysts in the oxidation of *trans* (Table 3, entries 7–12), with 100% selectivity for all of them, and with the highest conversions for the molybdenum catalysts (**MCM-MoBrL**<sub>2</sub> 100% and **MCM-MoIL**<sub>2</sub> 93%), while the tungsten ones exhibit conversions ranging from 19 to 56%. Again the molybdenum materials are more active than the respective complexes, while all the tungsten complexes become less active and less selective when grafted in **MCM**.

**MCM-MoBrL**<sub>2</sub> and **MCM-MoIL**<sub>2</sub> are again the most active catalysts in the oxidation of geraniol, with conversions of 98 and 100%, respectively, similar to those afforded by the complexes (Table 3, entries 13–18). The tungsten catalysts lead to lower conversions than the molybdenum materials and their corresponding complexes. In general, the heterogeneous catalysts are less selective toward the 2,3-oxirane product than the homogeneous ones, the 6,7-oxirane being formed in higher amounts.

The two molybdenum heterogeneous catalysts **MCM-MoXL**<sub>2</sub> (X = Br, I) lead to 100% conversions in the oxidation of *S*-limonene (Table 3 entries 23, 24), but the other materials are much less active (17–35%, Table 3, entries 19–22). However, **MCM-MoBrL**<sub>2</sub> is very selective toward the *E*-epoxide (88%), while **MCM-MoIL**<sub>2</sub> produces the same amount of the *Z*- and *E*-epoxides. The di-epoxide, formed by some homogeneous catalysts, is not observed. The activity of all the tungsten materials was lower than that of the complexes.

The oxidation of 1-octene was hard to achieve by the **MCM** materials (Table 3, entries 25–30), and both the conversions and the selectivity were in general very low.

In conclusion it is possible to say that the immobilization of the molybdenum complexes in **MCM** improved their capability as catalysts, making them more active and selective for most of the substrates tested. The tungsten complexes did not become better catalysts after their immobilization. The results of conversions and selectivity for the catalysts supported in **MCM** were lower or, in a few cases, similar to those obtained for the complexes.

It is interesting to note that the [Mo( $\eta^3$ -C<sub>3</sub>H<sub>5</sub>)X(CO)<sub>2</sub>(L)] complexes (L = L<sub>1</sub>, L<sub>2</sub>, and L<sub>3</sub>, respectively **1**, **2**, and **3**) [13] became less active after immobilization. However, the activity of molybdenum materials **MoBrL**<sub>1</sub> and **MoIL**<sub>1</sub>, described previously, increased after being supported in **MCM**.

Although tungsten complexes are good catalysts, they do not improve when they are supported and act as heterogeneous catalysts, and the same happens with the molybdenum complexes of the type [Mo( $\eta^3$ -C<sub>3</sub>H<sub>5</sub>)X(CO)<sub>2</sub>(L<sub>Y</sub>)] [13]. On the contrary, complexes [Mo(X)<sub>2</sub>(CO)<sub>3</sub>(L<sub>1</sub>)] [12] and [MoX<sub>2</sub>(CO)<sub>3</sub>(2-amino-1,3,4-thiadiazole)<sub>2</sub>] [16] become more active in **MCM**, while [WX<sub>2</sub>(CO)<sub>3</sub>(2-amino-1,3,4-thiadiazole)<sub>2</sub>] [16] increase their activity for X = I and decrease it for X = Br.

A quality of this kind of immobilized complexes is their recyclability and absence of leaching, which was studied previously in a series of functionalized materials. It was found that the conversions decreased by small amounts in five successive runs of the epoxidation of some of *trans*-

**Table 3**

Olefin epoxidation catalyzed with materials **MCM-WBrL<sub>1</sub>**, **MCM-WIL<sub>1</sub>**, **MCM-MoBrL<sub>2</sub>**, **MCM-MoIL<sub>2</sub>**, **MCM-WBrL<sub>2</sub>** and **MCM-WIL<sub>2</sub>**, of *cis*-hex-3-en-1-ol (*cis*), *trans*-hex-3-en-1-ol (*trans*), geraniol (*ger*), *S*-limonene (*lim*) and 1-octene (1-oct).

Entry	Substrate <sup>a</sup>	Catalyst	Conv. <sup>b</sup> %	Select. <sup>c</sup> %	Yield %
1	<i>cis</i> -hex-3-en-1-ol	<b>MCM-WBrL<sub>1</sub></b>	30	100	30
2		<b>MCM-WIL<sub>1</sub></b>	47	100	47
3		<b>MCM-WBrL<sub>2</sub></b>	21	100	21
4		<b>MCM-WIL<sub>2</sub></b>	40	100	40
5		<b>MCM-MoBrL<sub>2</sub></b>	100	100	100
6		<b>MCM-MoIL<sub>2</sub></b>	100	100	100
7	<i>trans</i> -hex-3-en-1-ol	<b>MCM-WBrL<sub>1</sub></b>	31	100	31
8		<b>MCM-WIL<sub>1</sub></b>	43	100	43
9		<b>MCM-WBrL<sub>2</sub></b>	19	100	19
10		<b>MCM-WIL<sub>2</sub></b>	56	100	56
11		<b>MCM-MoBrL<sub>2</sub></b>	100	100	100
12		<b>MCM-MoIL<sub>2</sub></b>	93	100	93
13	geraniol	<b>MCM-WBrL<sub>1</sub></b>	75	74	30/25 <sup>d</sup>
14		<b>MCM-WIL<sub>1</sub></b>	89	45	39/39 <sup>d</sup>
15		<b>MCM-WBrL<sub>2</sub></b>	85	77	50/15 <sup>d</sup>
16		<b>MCM-WIL<sub>2</sub></b>	58	98	37/20 <sup>d</sup>
17		<b>MCM-MoBrL<sub>2</sub></b>	98	98	70/28 <sup>d</sup>
18		<b>MCM-MoIL<sub>2</sub></b>	100	92	56/36 <sup>d</sup>
19	<i>S</i> -limonene	<b>MCM-WBrL<sub>1</sub></b>	25	86	10/12 <sup>e</sup>
20		<b>MCM-WIL<sub>1</sub></b>	17	61	5/5 <sup>e</sup>
21		<b>MCM-WBrL<sub>2</sub></b>	23	84	11/18 <sup>e</sup>
22		<b>MCM-WIL<sub>2</sub></b>	35	86	15/15 <sup>e</sup>
23		<b>MCM-MoBrL<sub>2</sub></b>	100	97	7/88 <sup>e</sup>
24		<b>MCM-MoIL<sub>2</sub></b>	100	98	45/46 <sup>e</sup>
25	1-octene	<b>MCM-WBrL<sub>1</sub></b>	16	11	2
26		<b>MCM-WIL<sub>1</sub></b>	9	45	4
27		<b>MCM-WBrL<sub>2</sub></b>	1	25	0.3
28		<b>MCM-WIL<sub>2</sub></b>	10	23	3
29		<b>MCM-MoBrL<sub>2</sub></b>	41	24	10
30		<b>MCM-MoIL<sub>2</sub></b>	25	22	6

<sup>a</sup> All reactions were carried out in dichloromethane in the presence of 2 eq. of oxidant (TBHP) and 175 mg of catalyst at 328 K; <sup>b</sup> Calculated after 24 h; <sup>c</sup> Calculated as "Yield of epoxide"/"Conversion"\*100%; <sup>d</sup> Yield of 2,3-/ 6,7-oxirane products; <sup>e</sup> Yield of Z-epoxide, E-epoxide.

hex-2-en-1-ol catalyzed by MoI<sub>2</sub>(CO)<sub>3</sub>(IMP) or MoBr(η<sup>3</sup>-C<sub>3</sub>H<sub>5</sub>)(CO)<sub>2</sub>(IMP) complexes immobilized in **MCM** in the presence of TBHP [25], and also by MoI<sub>2</sub>(CO)<sub>3</sub> complexes anchored in a helical **MCM** material by an asymmetric bidentate nitrogen ligand derived from 2-aminopyridine glycidylpropyl [26]. The Mo(CO<sub>3</sub>)I<sub>2</sub> complex of 2-(2'-hydroxyphenyl)imidazoline underwent a 20% deactivation in the epoxidation of *R*(+)-limonene, but after grafting a similar deactivation was only observed in the 3rd run [27]. These examples indicate that the immobilized Mo(II) precursors provide recyclable heterogeneous catalysts.

Leaching was also examined previously. For instance, the Mo(CO<sub>3</sub>)I<sub>2</sub> complex of 2-(2'-hydroxyphenyl)imidazoline grafted in **MCM** was applied to the epoxidation of *R*(+)-limonene. The solution was filtered after 2 h and the remaining solution showed no activity during the following 22 h, while without filtering, the heterogeneous catalyst remained active for a few hours [25]. The suspension containing the [Mo(η<sup>5</sup>-C<sub>3</sub>H<sub>5</sub>)Cl(CO)<sub>2</sub>(L<sub>1</sub>)] complex immobilized in **MCM** lost its activity in the epoxidation of *cis*-cyclooctene after removing the catalyst by filtration [12].

## 2.5. Catalytic studies. Mechanisms

The reaction mechanism should help to understand the catalysis results. Since the M(II) complexes and materials are catalyst precursors, the TBHP oxidant starts by oxidizing them to M(VI) species. This reaction has been well studied for the complex [Mo(II)(η<sup>5</sup>-C<sub>5</sub>H<sub>5</sub>)(CO)<sub>3</sub>(X)] (X = Cl or CH<sub>3</sub>), which is converted to [Mo(VI)(η<sup>5</sup>-C<sub>5</sub>H<sub>5</sub>)O<sub>2</sub>(X)], the catalyst. The latter complexes have been isolated and characterized, [14,28,29] and a complete computational study led to the identification of the active species [30,31]. The reaction mechanism of the alkene epoxidation was very similar to that proposed for the [Mo(VI)O<sub>2</sub>X<sub>2</sub>(N—N)] complex, with X = Cl, Br, CH<sub>3</sub>, and N—N = bidentate nitrogen ligand (see Figure S3) [32,33]. The complex [MoO<sub>2</sub>X<sub>2</sub>(N—N)] is the active Mo(VI) catalyst (A<sub>1</sub>). In the first step, the HOOR oxidant approaches the metal over the center of a triangular O—O—X face (Figure S3, top) to form a heptacoordinate intermediate [MoO(OH)(OOR)X<sub>2</sub>(N—N)] (B<sub>1</sub>), where the OH and OOR ligands are bound by a OH...H hydrogen bond (B<sub>1</sub>). The C=C bond adds to the Mo—O bond, forming a large metallacycle including the OH...H hydrogen bond (C<sub>1</sub>),



which breaks down into the epoxide, the ROH alcohol, and the regenerated catalyst [33]. In Figure S4, we show a similar catalytic cycle for the  $[\text{Mo}(\eta^5\text{-C}_5\text{H}_5)(\text{CO})_3(\text{X})]$  system in a simplified version. The first step is the oxidation of this Mo(II) complex to the active Mo(VI) species  $[\text{Mo}(\eta^5\text{-C}_5\text{H}_5)\text{O}_2(\text{X})]$  ( $\text{A}_2$ ), from which the catalysis proceeds, over intermediates  $\text{B}_2$  (OH activation of the HOOR oxidant) and  $\text{C}_2$  (alkene addition) [30,31,34]. These mechanisms have been reviewed [35,36].

The complexes  $[\text{Mo}(\eta^5\text{-C}_3\text{H}_5)\text{Cl}(\text{CO})_2(\text{N}-\text{N})]$  ( $\text{N}-\text{N}$  = 1,4-(4-chloro)phenyl-2,3-naphthalenediazabutadiene) behave differently in the presence of TBHP. IR spectroscopic analysis and elemental analysis suggested that the most likely Mo(VI) intermediate was the dimer  $[\{\text{MoO}_2\text{Cl}(\text{N}-\text{N})\}_2(\mu\text{-O})]$  ( $\text{A}_3$ ) [15]. The determination of the single crystal X-ray diffraction structure of the analogue  $[\{\text{MoO}_2\text{Cl}(\text{bpy}^*)\}_2(\mu\text{-O})]$  ( $\text{bpy}^*$  = 4,4'-di-*tert*-Bu-2,2'-bipyridine) [37] and a computational study [15] confirmed the nature of the catalyst. The M(II) precursor in the present study,  $[\text{MX}_2(\text{CO})_3(\text{L}_{1,2,3})]$  ( $\text{M}$  = W, Mo), where the allyl ligand is replaced by CO and X, should by analogy, be converted in the new catalyst  $[\{\text{MX}_2(\text{L}_{1,2,3})\}_2(\mu\text{-O})]^{2+}$  ( $\text{A}_4$ ), after loss of the carbonyl ligands. The proposed catalytic cycles, including the three more relevant intermediates (A, B, C), are shown in Figures S5 for the  $[\text{Mo}(\eta^5\text{-C}_3\text{H}_5)\text{X}(\text{CO})_2(\text{N}-\text{N})]$  catalysts ( $\text{A}_3$ ,  $\text{B}_3$ ,  $\text{C}_3$ ) and in Fig. 6 for the complexes  $[\text{MX}_2(\text{CO})_3(\text{L}_{1,2,3})]$  addressed in the present work ( $\text{A}_4$ ,  $\text{B}_4$ ,  $\text{C}_4$ ).

The activity of the catalysts was theoretically ascertained through DFT calculations [38] (ADF program [39–41], see Computational details). We started by analyzing the oxidation step, and calculated the electronic and Gibbs energy of the oxidation reaction for the four  $[\text{MX}_2(\text{CO})_3(\text{L}_{1,2,3})]$  systems (W, Mo; Br, I) and compared them with the related  $[\text{Mo}(\eta^5\text{-C}_3\text{H}_5)\text{Cl}(\text{CO})_2(\text{N}-\text{N})]$  systems shown in Fig. S5. The

oxidation of the allyl complexes is much less exergonic than that of the other ones, with Gibbs energies ranging between  $\sim -74$  and  $-117$  kcal  $\text{mol}^{-1}$ , and  $\sim -259$  and  $-292$  kcal  $\text{mol}^{-1}$ , respectively, but this results from the different nature of the complexes and their products (the energy values are collected in Table S3, SI). On the other hand, the tungsten complexes are easier to oxidize than the molybdenum ones, by  $\sim 20$ – $25$  kcal  $\text{mol}^{-1}$ , reflecting the lower ionization energy of W compared to Mo, and the differences between Br and I derivatives are smaller, though reaction of iodides are more exergonic. However, the catalytic cycles must also be considered.

The catalytic cycles are shown in Fig. 6, and S3–S5. Only the three structures of intermediates A, B, and C were calculated for all systems. A set of structures of all the intermediates is shown in Fig. 7 for  $[\text{M}(\text{CO})_3(\text{L}_1)]$  and in Figure S6 for  $[\text{Mo}(\eta^5\text{-C}_3\text{H}_5)\text{Br}(\text{CO})_2(\text{L}_1)]$  and all their derivatives. The others are extremely similar. The determination of transition states was not attempted, owing the size of the binuclear complexes.

The more deeply studied reactions of the Mo(VI) mononuclear catalysts show very clearly that the step with the largest barrier corresponds to the  $\text{B} \rightarrow \text{C}$  conversion. It involves the entropy unfavored addition of the  $\text{C}=\text{C}$  bond of the alkene to the Mo–O(OR) bond of B (see Figures S3 and S4). C is the intermediate with the highest energy and gives rise to the products and the regenerated catalyst. The relative energies of the three tungsten and molybdenum intermediates addressed in this work are collected in Table 4. The intermediate C always has the highest energy and by comparison with previous systems [30,31,33] it may be inferred that the activation barriers associated with the formation of C and its decomposition will be slightly higher than the energy of

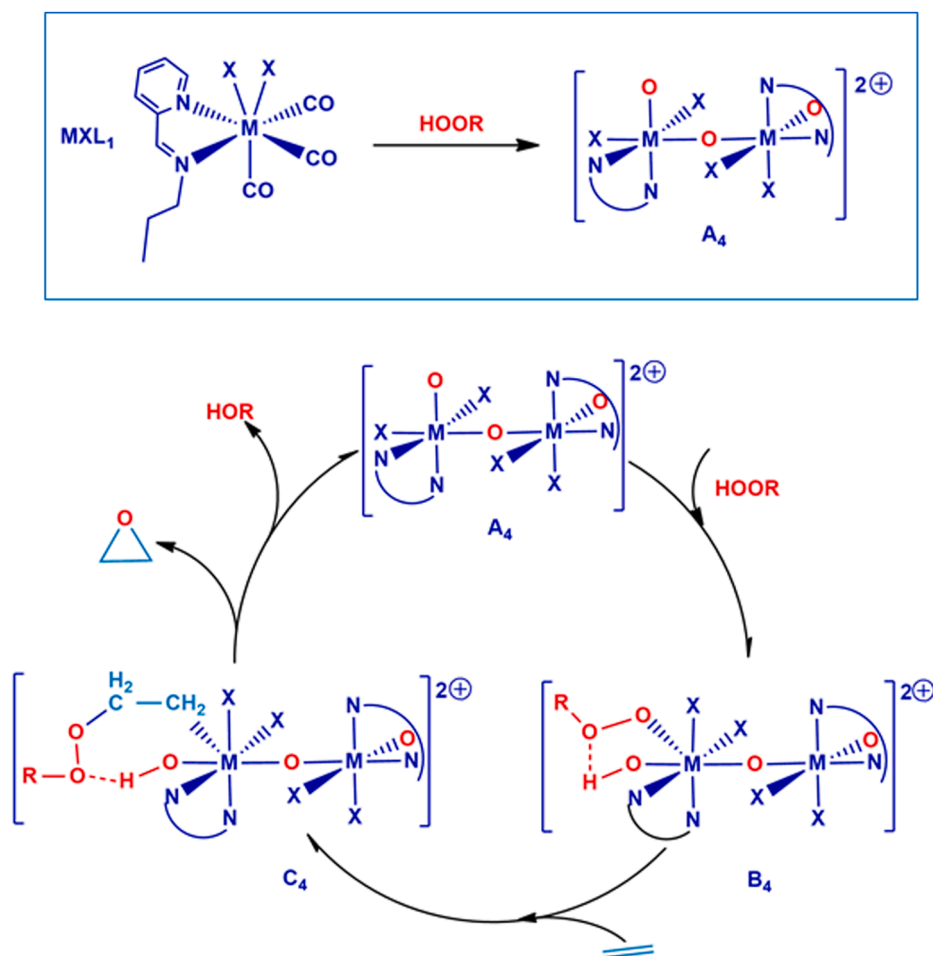


**Fig. 6.** Simplified mechanism of alkene epoxidation with HOOR by the  $[\{\text{MoX}_2(\text{L}_1)\}_2(\mu\text{-O})]^{2+}$  catalyst ( $\text{A}_4$ ). The oxidation of  $[\text{MX}_2(\text{CO})_3(\text{L}_{1,2,3})]$  ( $\text{M}$  = W, Mo;  $\text{X}$  = Br, I) to  $\text{A}_4$  by HOOR is shown in the top rectangle.

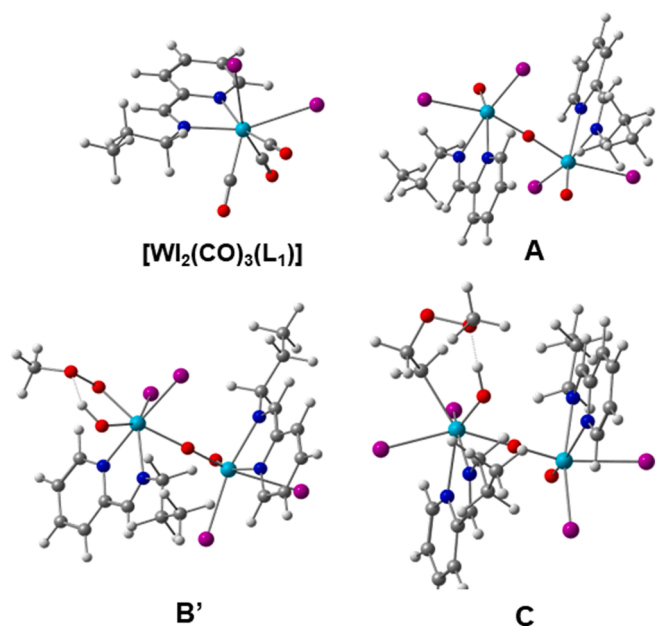


Fig. 7. Three dimensional structures of complex  $[Wl_2(CO)_3(L_1)]$ , the dimer formed upon oxidation by HOOR (A), the binuclear species resulting from OH activation of HOOR (B'), and the binuclear complex formed after addition of ethylene to B.

C. These energies of C are higher for the iodide complexes than the bromide ones, so that their higher activity must be associated with the previous oxidation reaction. Two different intermediates of type B intermediate (B and B') with a O—H...O hydrogen bond, differing by their orientation relative to the M—O—M line, were found for the allyl system with Br (Fig S6). B, with a Br—Mo—O—Mo—Br axis, is more stable than B' with a Br—Mo—O—Mo—OH one. However, a type B intermediate could not be obtained for the iodides. In all the iodides, the second intermediate is B' as shown in Fig. 7 for the  $[Wl_2(CO)_3(L_1)]$  system (notice the I—W—O—W—OH line).

The Gibbs energies are much higher than the electronic energies, because the two reactions, the OH activation of the ROOH oxidant and the addition of ethylene to the Mo—O bond, are both associative. The values are extremely similar for all complexes, even more than the energies, in this model system where the substrate was ethylene and the oxidant MeOOH. This helps to explain the apparent random results and the absence of a well defined pattern.

### 3. Conclusions

A family of  $[MX_2(CO)_3(L_Y)]$  complexes ( $MXL_Y$ : M = W, Mo; X = Br, I;  $L_Y = L_{1-3}$ , Scheme 2) was prepared and some of them immobilized in MCM. Complexes  $[WX_2(CO)_3(L_1)]$  (X = Br,  $WBrL_1$  and X = I,  $Wl_2L_1$ ) were structurally characterized by single crystal X-ray diffraction. To the best of our knowledge, these are the first examples of tungsten

complexes of this type and also of their immobilization in MCM materials.

We studied the catalytic activity of these complexes and materials in the oxidation of *cis*-hex-3-en-1-ol (*cis*), *trans*-hex-3-en-1-ol (*trans*), geraniol (*ger*), *S*-limonene (*lim*) and 1-octene (1-oct), with TBHP. The complexes studied here were in general less active in the oxidation of *trans* than  $[Mo(\eta^3-C_3H_5)X(CO)_2(L_Y)]$  (L =  $L_1$ ,  $L_2$ , and  $L_3$ , respectively 1, 2, and 3) [13], which oxidized this substrate with 99% conversion and 100% selectivity. Complex 2 was more selective than  $MoBrL_2$  for the epoxidation of *trans*, but  $MoIL_3$ , on the other hand, converted *trans* with much higher selectivity and conversion than complex 3. The two families behaved similarly in the oxidation of *ger* (very active) and 1-octene (poorly).

DFT calculations suggested that the iodide complexes were more easily oxidized by ROOH, but the catalytic reaction was less favored than for bromides. This and the very close energies found for the catalytic reaction prevent us from drawing reliable conclusions.

The immobilization of the molybdenum complexes  $MXL_Y$  in MCM made them more active and selective for most of the substrates tested (also  $MXL_1$  with other substrates). The opposite, however, happened with the tungsten complexes, as the conversions and selectivity for the catalysts supported in MCM were lower or, in a few cases, similar to those obtained for the complexes.

Although tungsten complexes are good catalysts, they do not become better when supported in MCM. Since their synthesis is more difficult than the synthesis of the molybdenum analogues, they do not prove to be very promising. Some of the molybdenum heterogeneous catalysts are more active than the complexes and share the advantages of heterogeneous catalysts.

### 4. Experimental

#### 4.1. General considerations

All reagents were obtained from Aldrich and used as received. All the work involving sensitive compounds was carried out using standard Schlenk techniques. Commercial-grade solvents were dried and deoxygenated by standard procedures (i.e., toluene over Na/benzophenone ketyl, dichloromethane and hexane over  $CaH_2$ ), distilled under nitrogen, and kept over 4 Å molecular sieves.

The organometallic complexes  $[MX_2(CH_3CN)_2(CO)_3]$  (M = Mo, X = I, Br; M = W, X = I, X = Br) were prepared as described before [42,43]. Ligands  $C_5H_4NCY = N(CH_2)_2CH_3$  (Y = H,  $L_1$ ; Y =  $CH_3$ ,  $L_2$ ; Y = Ph,  $L_3$ ) and  $C_5H_4NCY = N(CH_2)_3Si(OEt)_3$  (Y = H,  $L_1Si$ ; Y =  $CH_3$ ,  $L_2Si$ ) were also prepared as reported [12]. MCM-41 and post synthetic derivatized materials were obtained as described previously, using  $[(C_{16}H_{33})N(CH_3)_3]Br$  (CTAB) as the templating agent [13,18]. Physisorbed water was removed (540 °C for six hours under air) from calcined MCM-41 before the grafting experiment, by heating at 180 °C in vacuum ( $10^{-2}$  Pa) during two hours. Hybrid materials were prepared using ligands  $L_1Si$  and  $L_2Si$  as reported, with an organic material load of  $\approx 3\%$  [12,44,45].

FTIR spectra were obtained as KBr pellets and diffuse reflectance measurements (DRIFT) on a Nicolet 6700 in the 400–4000  $cm^{-1}$  range

Table 4

Calculated relative energies and Gibbs energies (kcal mol<sup>-1</sup>) for the A, B, and C intermediates in the catalytic epoxidation of ethylene with MeOOH.

Initial complex	$\Delta E$				$\Delta G$			
	A	B	B'	C	A	B	B'	C
$[WBr_2(CO)_3(L_1)]$	0	9.94		20.82	0	25.14		50.59
$[Wl_2(CO)_3(L_1)]$	0		15.79	24.90	0		30.55	54.95
$[MoBr_2(CO)_3(L_1)]$	0	11.9		18.92	0	26.86		47.79
$[Mol_2(CO)_3(L_1)]$	0		16.17	23.79	0		30.98	54.49
$[W(\eta^3-C_3H_5)Br(CO)_2(L_1)]$	0	8.94	9.79	23.99	0	24.03	25.81	53.99
$[W(\eta^3-C_3H_5)I(CO)_2(L_1)]$	0	9.20		25.45	0	23.59		55.4
$[Mo(\eta^3-C_3H_5)Br(CO)_2(L_1)]$	0	10.68	12.31	24.07	0	25.67	28.1	54.11
$[Mo(\eta^3-C_3H_5)I(CO)_2(L_1)]$	0	10.78		25.14	0	25.67		54.11

( $\text{cm}^{-1}$  resolution). Powder XRD measurements were taken on a Philips Analytical PW 3050/60 X'Pert PRO ( $\theta/2\theta$ ) equipped with X'Celerator detector and with automatic data acquisition (X'Pert Data Collector (v2.0b) software), using a monochromatic Cu K $\alpha$  radiation as the incident beam, operating at 40 kV–30 mA. XRD diffraction patterns were obtained by continuous scanning in a  $2\theta$  range of 2 to  $10^\circ$  with  $2\theta$  step size of  $0.017^\circ$  and a scan step time of 99.695 s.  $^1\text{H}$  and  $^{13}\text{C}$  solution NMR spectra were obtained with a Bruker Avance 400 spectrometer.  $^{29}\text{Si}$  and  $^{13}\text{C}$  solid state NMR spectra were performed at University of Aveiro by Dr Paula Ferreira, and were recorded at 79.49 MHz and 100.62 MHz, respectively, on a (9.4 T) Bruker Avance 400P spectrometer.  $^{29}\text{Si}$  CP MAS NMR spectra were recorded with 5.5  $\mu\text{s}$  1H  $90^\circ$  pulse, 2 ms contact time, a spinning rate of 8 kHz, and 4 s recycle delays. Chemical shifts are quoted in ppm from TMS.  $^{13}\text{C}$  spectra (solid state) were recorded at 125.76 MHz on a Bruker Avance 500 spectrometer. The  $\text{N}_2$  sorption measurements were obtained in an automatic apparatus (ASAP 2010; Micrometrics). BET specific surface areas ( $S_{\text{BET}}$ ,  $p/p_0$  from 0.03 to 0.13) and specific total pore volume,  $V_p$  were estimated from  $\text{N}_2$  adsorption isotherms measured at 77 K. The pore size distribution (PSD) was calculated by the BJH method using the modified Kelvin equation, with correction for the statistical film thickness on the pore walls [23]. The statistical film thickness was calculated using the Harkins-Jura equation in the  $p/p_0$  range from 0.1 to 0.95. Microanalyses (C, N, H) and ICP analyses for determination of molybdenum and tungsten were performed at the University of Vigo.

#### 4.2. Catalytic tests

The complexes and materials were tested in epoxidation of multifunctional olefins, *cis*-hex-3-en-1-ol (*cis*), *trans*-hex-3-en-1-ol (*trans*), geraniol (*ger*), *S*-limonene (*lim*) and 1-octene (1-oct), using *tert*-butylhydroperoxide (TBHP) as oxidant (5.5 M in *n*-decane). The catalytic oxidation tests were carried out at 328 K, using dichloromethane as solvent. The reactions occurred under air in a reaction vessel equipped with a magnetic stirrer and a condenser. In a typical experiment, the vessel was loaded with catalyst (1 mol% for complexes and 175 mg for materials), olefin (100 mol%), oxidant (200 mol%) and 3 mL of solvent. The final volume of the reaction was ca. 6 mL. The addition of the oxidant determined the initial time of the reaction. Conversion, product yields and stereochemistry were monitored by sampling periodically and analyzing the products on a Shimadzu QP2010-Plus GC/MS system and a capillary column (Teknokroma TRB- 5MS, TRB-1MS) operating in the linear velocity mode.

#### 4.3. Synthesis of complexes

##### 4.3.1. $[\text{WX}_2(\text{CO})_3\{\text{C}_5\text{H}_4\text{NCH} = \text{N}(\text{CH}_2)_2\text{CH}_3\}]$ ( $\text{X} = \text{Br}, \text{I}$ )

A solution of  $[\text{WX}_2(\text{CO})_3(\text{CH}_3\text{CN})_2]$  ( $\text{X} = \text{I}, \text{Br}$ ) (1 mmol) in dichloromethane (10 mL) was added to a solution of the ligand  $\text{C}_5\text{H}_4\text{NCH} = \text{N}(\text{CH}_2)_2\text{CH}_3$  (**L**<sub>1</sub>, 1.2 mmol, 0.178 g) in dichloromethane (10 mL). The resulting mixture was stirred for 6 h at room temperature and under a nitrogen atmosphere. The solution was filtered and concentrated by evaporation, and pentane was added. The precipitate was filtered, and the product dried under vacuum.

##### 4.3.1.1. $[\text{WBr}_2(\text{CO})_3\{\text{C}_5\text{H}_4\text{NCH} = \text{N}(\text{CH}_2)_2\text{CH}_3\}]$ (**WBrL**<sub>1</sub>). Yield ( $\eta$ ): 88% (0.51 g) (orange-brick powder)

Elemental analysis  $\text{WBr}_2\text{C}_{12}\text{H}_{12}\text{N}_2\text{O}_3$  (575.9) (%): Calc C 25.03, N 4.86, H 2.10; found C 25.64, N 4.40, H 2.52.

IR (KBr pellets,  $\nu \text{ cm}^{-1}$ ): 3069 (m), 3022 (w), 2971 (m), 2942 (w), 2921 (m), 2878 (w), 2036 (vs), 1956 (vs), 1904 (vs), 1621 (m), 1595 (m), 1477 (s), 1309 (m), 1261 (m), 1242 (m), 782 (s), 543 (s), 490 (s).

$^1\text{H}$  NMR (400.13 MHz,  $(\text{CD}_3)_2\text{CO}$ , room temp., ppm): 1.03 (t, 3H,  $\text{H}_1$ ), 1.87 (m, 2H,  $\text{H}_2$ ), 3.14 (t, 2H,  $\text{H}_3$ ), 7.91 (t, 1H,  $\text{H}_8$ ), 8.43 (t, 1H,  $\text{H}_7$ ), 8.52 (t, 1H,  $\text{H}_6$ ), 8.97 (d, 1H,  $\text{H}_9$ ), 9.37 (s, 1H,  $\text{H}_4$ ) ppm.

$^{13}\text{C}\{^1\text{H}\}$  NMR (400.13 MHz,  $(\text{CD}_3)_2\text{CO}$ , room temp., ppm): 10.2 (C1), 20.7 (C2), 41.9 (C3), 122.1 (C8), 128.6 (C7), 137.7 (C6), 150.3 (C9), 165.8 (C4), 184.7 (CO) 194.4 (CO).

##### 4.3.1.2. $[\text{WI}_2(\text{CO})_3\{\text{C}_5\text{H}_4\text{NCH} = \text{N}(\text{CH}_2)_2\text{CH}_3\}]$ (**WIL**<sub>1</sub>). Yield ( $\eta$ ): 98% (0.66 g) (red powder),

Elemental analysis  $\text{WI}_2\text{C}_{12}\text{H}_{12}\text{N}_2\text{O}_3$  (669.9) (%): Calc C 21.52, N 4.18, H 1.81; found: C 21.65, N 4.31, H 2.08.

IR (KBr pellets,  $\nu \text{ cm}^{-1}$ ): 3071 (w), 3016 (w), 2972 (m), 2969 (m), 2933 (w), 2885 (m), 2014 (vs), 1935 (vs), 1896 (vs), 1617 (m), 1595 (m), 1554 (w), 1480 (s), 1391 (m), 1310 (s), 1260 (m), 1239 (m), 1159 (m), 770 (vs), 754 (s), 519 (s), 494 (s)  $\text{cm}^{-1}$ .

$^1\text{H}$  NMR (400.13 MHz,  $(\text{CD}_3)_2\text{CO}$ , room temp., ppm): 1.05 (t, 3H,  $\text{H}_1$ ), 2.05 (m, 2H,  $\text{H}_2$ ), 4.46 (t, 2H,  $\text{H}_3$ ), 7.88 (t, 1H,  $\text{H}_8$ ), 8.41 (t, 1H,  $\text{H}_7$ ), 8.51 (t, 1H,  $\text{H}_6$ ), 9.33 (s, 1H,  $\text{H}_4$ ), 9.81 (d, 1H,  $\text{H}_9$ ).

$^{13}\text{C}\{^1\text{H}\}$  NMR (400.13 MHz,  $(\text{CD}_3)_2\text{CO}$ , room temp., ppm): 10.3 (C1), 24.4 (C2), 67.4 (C3), 128.0 (C8), 130.3 (C7), 140.4 (C6), 155.4 (C9), 168.2 (C4).

##### 4.3.2. $[\text{MX}_2(\text{CO})_3\{\text{C}_5\text{H}_4\text{NCCH}_3 = \text{N}(\text{CH}_2)_2\text{CH}_3\}]$ ( $\text{M} = \text{W}, \text{Mo}$ and $\text{X} = \text{I}, \text{Br}$ )

A solution of  $[\text{MX}_2(\text{CO})_3(\text{CH}_3\text{CN})_2]$  ( $\text{M} = \text{W}, \text{Mo}$  and  $\text{X} = \text{I}, \text{Br}$ ) (0.5 mmol) in dichloromethane (10 mL) was added to a solution of the ligand  $\text{C}_5\text{H}_4\text{NCCH}_3 = \text{N}(\text{CH}_2)_2\text{CH}_3$  (**L**<sub>2</sub>, 1.2 mmol, 0.195 g) also in dichloromethane (10 mL). The resulting mixture was stirred for 4 h (tungsten) or 6 h (molybdenum) at room temperature and under a nitrogen atmosphere. The solution was filtered and concentrated to a solid. After filtration, the product was recrystallized from hexane.

##### 4.3.2.1. $[\text{WBr}_2(\text{CO})_3\{\text{C}_5\text{H}_4\text{NCCH}_3 = \text{N}(\text{CH}_2)_2\text{CH}_3\}]$ (**WBrL**<sub>2</sub>). Yield ( $\eta$ ): 80% (0.47 g) (red powder)

Elemental analysis  $\text{WBr}_2\text{C}_{13}\text{H}_{14}\text{N}_2\text{O}_3$  (589.92) (%): Calc: C 26.47, N 4.75, H 2.39 found: C 26.13, N 4.59, H 2.03.

IR (KBr pellets,  $\nu \text{ cm}^{-1}$ ): 3411 (s), 3046 (m), 2960 (s), 2932 (s), 2874 (m), 2033 (vs), 1949 (vs), 1902 (vs), 1619 (s), 1603 (s), 1530 (m) 1435 (s), 1383 (m), 1260 (m), 1163 (m), 1093 (m), 1049 (m), 1026 (w), 951 (m), 779 (s), 750 (s).

$^1\text{H}$  NMR (400.13 MHz,  $\text{CDCl}_3$ , room temp., ppm): 1.06 (t, 3H,  $\text{H}_1$ ), 2.13 (t, 2H,  $\text{H}_2$ ), 2.69 (s, 3H,  $\text{H}_{10}$ ) 3.84 (t, 2H,  $\text{H}_3$ ), 7.92 (t, 1H,  $\text{H}_8$ ), 8.20 (d, 1H,  $\text{H}_6$ ), 8.35 (t, 1H,  $\text{H}_7$ ), 8.76 (d, 1H,  $\text{H}_9$ ).

$^{13}\text{C}\{^1\text{H}\}$  NMR (400.13 MHz,  $\text{CDCl}_3$ , room temp., ppm): 12.1 (C1), 14.9 (C2), 23.7 (C10), 54.2 (C3), 124.5 (C8), 128.3 (C6), 141.8 (C7), 149.1 (C9), 149.9 (C5), 167.2 (C4).

##### 4.3.2.2. $[\text{WI}_2(\text{CO})_3\{\text{C}_5\text{H}_4\text{NCCH}_3 = \text{N}(\text{CH}_2)_2\text{CH}_3\}]$ (**WIL**<sub>2</sub>). Yield ( $\eta$ ): 88% (0.60 g) (purple powder)

Elemental analysis  $\text{WI}_2\text{C}_{13}\text{H}_{14}\text{N}_2\text{O}_3$  (683.92) (%): Calc C 22.83, N 4.10, H 2.06 found: C 22.77, N 3.81, H 1.88.

IR (KBr pellets,  $\nu \text{ cm}^{-1}$ ): 3421 (s), 3041 (m), 2966 (m), 2903 (m), 2873 (w), 2065 (m), 2019 (s), 2003 (m), 1925 (vs), 1654 (m), 1605 (m), 1528 (m), 1488 (w), 1457 (s), 1384 (m), 1305 (m), 1227 (m), 1162 (m), 1092 (w), 1027 (w), 946 (w), 776 (s), 732 (s).

$^1\text{H}$  NMR (400.13 MHz,  $(\text{CD}_3)_2\text{CO}$ , room temp., ppm): 1.08 (t, 3H,  $\text{H}_1$ ), 2.10 (s, 3H,  $\text{H}_{10}$ ), 2.85 (t, 2H,  $\text{H}_2$ ) 3.78 (t, 2H,  $\text{H}_3$ ), 7.82 (t, 1H,  $\text{H}_8$ ), 8.40 (d, 1H,  $\text{H}_6$ ), 8.52 (t, 1H,  $\text{H}_7$ ), 9.56 (d, 1H,  $\text{H}_9$ ).

$^{13}\text{C}\{^1\text{H}\}$  NMR (400.13 MHz,  $\text{CDCl}_3$ , room temp., ppm): 13.2 (C1), 22.9 (C2), 27.7 (C10), 44.0 (C3), 123.6 (C8), 128.8 (C6), 138.8 (C7), 151.0 (C9), 203.2 (CO), 209.3 (CO).

##### 4.3.2.3. $[\text{MoBr}_2(\text{CO})_3\{\text{C}_5\text{H}_4\text{NCCH}_3 = \text{N}(\text{CH}_2)_2\text{CH}_3\}]$ (**MoBrL**<sub>2</sub>). Yield ( $\eta$ ): 93% (0.47 g) (red powder)

Elemental analysis  $\text{MoBr}_2\text{C}_{13}\text{H}_{14}\text{N}_2\text{O}_3$  (502.01) (%): Calc: C 31.10, N 5.58, H 2.81 found: C 29.98, N 5.23, H 2.51.

IR (KBr pellets,  $\nu \text{ cm}^{-1}$ ): 3440 (s) 3070 (m), 3028 (m), 2964 (m), 2930 (m), 2873 (w), 2044 (m), 1971 (vs), 1921 (s), 1901 (m), 1617 (s),

1531 (w), 1472 (m), 1477 (m), 1435 (m), 1305 (w), 1250 (w), 1164 (w), 1092 (w), 1023 (w), 945 (m), 776 (s), 748 (s).

$^1\text{H}$  NMR (400.13 MHz,  $(\text{CD}_3)_2\text{CO}$ , room temp., ppm): 1.21 (t, 3H,  $\text{H}_1$ ), 2.20 (s, 2H,  $\text{H}_{10}$ ), 2.67 (d, 3H,  $\text{H}_2$ ), 4.64 (t, 2H,  $\text{H}_3$ ), 8.21 (t, 1H,  $\text{H}_8$ ), 8.45 (t, 1H,  $\text{H}_6$ ), 8.57 (d, 1H,  $\text{H}_7$ ), 9.26 (d, 1H,  $\text{H}_9$ ).

$^{13}\text{C}\{^1\text{H}\}$  NMR (400.13 MHz,  $(\text{CD}_3)_2\text{CO}$ , room temp., ppm): 13.7 (C1), 18.1 (C2), 24.6 (C10), 55.0 (C3), 121.3 (C8), 124.7 (C6), 136.1 (C7), 148.8 (C9), 158.3 (C5), 166.2 (C4).

**4.3.2.4.  $[\text{MoI}_2(\text{CO})_3\text{C}_5\text{H}_4\text{NCCH}_3 = \text{N}(\text{CH}_2)_2\text{CH}_3]$  ( $\text{MoIL}_2$ ). Yield ( $\eta$ ): 91% (0.54 g) (red-wine powder)**

Elemental analysis  $\text{MoI}_2\text{C}_{13}\text{H}_{14}\text{N}_2\text{O}_3$  (596.01) (%): Calc: C 26.20, N 4.70, H 2.37. found: C 26.09, N 4.45, H 2.01.

IR (KBr pellets,  $\nu \text{ cm}^{-1}$ ): 3415 (s), 3077 (m), 2990 (m), 2964 (m), 2905 (w), 2872 (w), 2012 (m), 1963 (vs), 1920 (vs), 1850 (m) 1616 (m) 1593 (m), 1433 (m), 1375 (m), 1302 (w), 1250 (m), 1162 (m), 1096 (w), 1021 (w), 994 (w) 945 (w), 774 (s), 746 (s).

$^1\text{H}$  NMR (400.13 MHz,  $(\text{CD}_3)_2\text{CO}$ , room temp., ppm): 1.07 (t, 3H,  $\text{H}_1$ ), 2.01 (s, 3H,  $\text{H}_{10}$ ), 2.73 (d, 2H,  $\text{H}_2$ ), 4.48 (t, 2H,  $\text{H}_3$ ), 7.93 (t, 1H,  $\text{H}_8$ ), 8.46 (t, 1H,  $\text{H}_6$ ), 8.52 (d, 1H,  $\text{H}_7$ ), 9.68 (d, 1H,  $\text{H}_9$ ).

$^{13}\text{C}\{^1\text{H}\}$  NMR (400.13 MHz,  $(\text{CD}_3)_2\text{CO}$ , room temp., ppm): 10.9 (C1), 14.7 (C2), 21.0 (C10), 53.9 (C3), 127.9 (C8), 130.8 (C6), 132.6 (C7), 137.4 (C9), 148.3 (C5).

**4.3.3.  $[\text{MX}_2(\text{CO})_3\{\text{C}_5\text{H}_4\text{NC}_6\text{H}_5 = \text{N}(\text{CH}_2)_2\text{CH}_3\}]$  ( $\text{M} = \text{W}$ ,  $\text{Mo}$  and  $\text{X} = \text{I}$ )**

A solution of  $[\text{MX}_2(\text{CO})_3(\text{CH}_3\text{CN})_2]$  ( $\text{M} = \text{W}$ ,  $\text{Mo}$  and  $\text{X} = \text{I}$ ,  $\text{Br}$ ) (0.5 mmol) in dichloromethane (10 mL) was added to a solution of the ligand  $\text{C}_5\text{H}_4\text{NCCH}_3 = \text{N}(\text{CH}_2)_2\text{CH}_3$  ( $\text{L}_3$ , 1.2 mmol, 0.270 g) also in dichloromethane (10 mL). The resulting mixture was allowed to stir for 4 h (tungsten) or 6 h (molybdenum) at room temperature and under a nitrogen atmosphere. The solution was then filtered and concentrated by evaporation. The product was filtered and recrystallized with hexane and dried under vacuum.

**4.3.3.1.  $\text{WBr}_2(\text{CO})_3\text{C}_5\text{H}_4\text{NCPH} = \text{N}(\text{CH}_2)_2\text{CH}_3]$  ( $\text{WBrL}_3$ ). Yield ( $\eta$ ): 77% (0.50 g) (black crystalline powder)**

Elemental analysis  $\text{WBr}_2\text{C}_{18}\text{H}_{16}\text{N}_2\text{O}_3$  (652.00) (%): Calc: C 33.16, N 4.30, H 2.47; found: C 33.07, N 4.19, H 2.34.

IR (KBr pellets,  $\nu \text{ cm}^{-1}$ ): 3092 (w), 3056 (s), 2966 (s), 2872 (m), 2083 (w), 2036 (vs), 1956 (vs), 1910 (s), 1671 (s), 1607 (s), 1525 (m), 1449 (s), 1347 (m), 1286 (s), 1226 (w), 1163 (w), 1160 (w), 1054 (m), 949 (s), 812 (m), 770 (s), 698 (s), 646 (m).

$^1\text{H}$  NMR (400.13 MHz,  $(\text{CD}_3)_2\text{CO}$ , room temp., ppm): 1.02 (t, 3H,  $\text{H}_1$ ), 1.88 (t, 2H,  $\text{H}_2$ ), 3.03 (m, 2H,  $\text{H}_3$ ), 7.63 (dd, 2H,  $\text{H}_{12}$   $\text{H}_{14}$ ), 7.79 (t, 1H,  $\text{H}_{13}$ ), 8.06 (dd, 2H,  $\text{H}_{11}$   $\text{H}_{15}$ ), 8.33 (t, 1H,  $\text{H}_8$ ), 8.44 (d, 1H,  $\text{H}_6$ ), 8.77 (t, 1H,  $\text{H}_7$ ), 9.23 (d, 1H,  $\text{H}_9$ ).

$^{13}\text{C}\{^1\text{H}\}$  NMR (400.13 MHz,  $(\text{CD}_3)_2\text{CO}$ , room temp., ppm): 10.5 (C1), 20.5 (C2), 40.8 (C3), 127.0 (C6), 128.8 (C12 C14), 129.2 (C8), 130.7 (C11 C15), 134.2 (C13), 143.9 (C7), 145.2 (C9), 148.6 (C4), 189.0 (CO).

**4.3.3.2.  $[\text{WI}_2(\text{CO})_3\text{C}_5\text{H}_4\text{NCPH} = \text{N}(\text{CH}_2)_2\text{CH}_3]$  ( $\text{WIL}_3$ ). Yield ( $\eta$ ): 72% (0.54 g) (dark-blue powder)**

Elemental analysis  $\text{WI}_2\text{C}_{18}\text{H}_{16}\text{N}_2\text{O}_3$  (746.00) (%): Calc: C 28.98, N 3.76, H 2.16; found: C 28.71, N 3.57, H 1.92.

IR (KBr pellets,  $\nu \text{ cm}^{-1}$ ): 3041 (w), 3028 (w) 2964 (w), 2928 (m), 2852 (w), 2002 (m), 1949 (s), 1919 (s), 1663 (m), 1567 (s), 1444 (m), 1385 (w), 1281 (w), 1187 (w), 1054 (w), 1028 (m), 942 (m), 864 (m), 768 (s), 699 (s).

$^1\text{H}$  NMR (400.13 MHz,  $(\text{CD}_3)_2\text{CO}$ , room temp., ppm): 1.05 (t, 3H,  $\text{H}_1$ ), 1.91 (t, 2H,  $\text{H}_2$ ), 3.22 (m, 2H,  $\text{H}_3$ ), 7.27 (dd, 2H,  $\text{H}_{12}$ ), 7.38 (m, 1H,  $\text{H}_{14}$ ), 7.55 (m, 2H,  $\text{H}_{11}$   $\text{H}_{15}$ ), 7.67 (m, 1H,  $\text{H}_8$ ), 7.76 ( $\text{H}_{13}$ ), 8.06 (t, 1H,  $\text{H}_7$ ), 8.09 (d, 1H,  $\text{H}_6$ ), 8.74 (d, 1H,  $\text{H}_9$ ).

$^{13}\text{C}\{^1\text{H}\}$  NMR (400.13 MHz,  $(\text{CD}_3)_2\text{CO}$ , room temp., ppm): 10.3

(C1), 20.7 (C2), 54.1 (C3), 124.3 (C12), 126.5 (C14), 128.0 (C11 C15), 129.5 (C8), 130.8 (C13), 132.7 (C7), 137.4 (C6), 148.4 (C9).

**4.3.3.3.  $[\text{MoBr}_2(\text{CO})_3\text{C}_5\text{H}_4\text{NCPH} = \text{N}(\text{CH}_2)_2\text{CH}_3]$  ( $\text{MoBrL}_3$ ). Yield ( $\eta$ ): 76% (0.43 g) (green powder)**

Elemental analysis  $\text{MoBr}_2\text{C}_{18}\text{H}_{16}\text{N}_2\text{O}_3$  (564.08) (%): Calc: C 38.33, N 4.97, H 2.86; found: C 38.16, N 4.42, H 2.71.

IR (KBr pellets,  $\nu \text{ cm}^{-1}$ ): 3073 (w), 3019 (w), 2965 (m), 2919 (m), 2874 (m), 2040 (s), 1967 (vs), 1918 (s), 1660 (m), 1594 (s), 1522 (m), 1449 (s), 1281 (m), 1162 (m), 1093 (w), 1018 (w), 940 (s), 775 (s), 695 (s).

$^1\text{H}$  NMR (400.13 MHz,  $(\text{CD}_3)_2\text{CO}$ , room temp., ppm): 1.05 (t, 3H,  $\text{H}_1$ ), 1.90 (t, 2H,  $\text{H}_2$ ), 3.01 (m, 2H,  $\text{H}_3$ ), 7.41 (dd, 2H,  $\text{H}_{12}$   $\text{H}_{14}$ ), 7.56 (m, 2H,  $\text{H}_{11}$   $\text{H}_{15}$ ), 7.68 (m, 1H,  $\text{H}_8$ ), 7.73 (d, 1H,  $\text{H}_{13}$ ), 8.14 (t, 1H,  $\text{H}_7$ ), 8.77 (m, 1H,  $\text{H}_6$ ), 9.53 (d, 1H,  $\text{H}_9$ ).

$^{13}\text{C}\{^1\text{H}\}$  NMR (400.13 MHz,  $(\text{CD}_3)_2\text{CO}$ , room temp., ppm): 11.4 (C1), 22.8 (C2), 39.6 (C3), 124.4 (C12), 126.9 (C14), 127.9 (C11), 129.5 (C15), 130.8 (C8), 132.6 (C13), 136.4 (C7), 138.2 (C6), 143.8 (C10), 148.5 (C9), 154.1 (C4), 154.6 (C5), 192.8 (CO).

**4.3.3.4.  $[\text{MoI}_2(\text{CO})_3\text{C}_5\text{H}_4\text{NCPH} = \text{N}(\text{CH}_2)_2\text{CH}_3]$  ( $\text{MoIL}_3$ ). Yield ( $\eta$ ): 87% (0.57 g) (dark-green powder)**

Elemental analysis  $\text{MoI}_2\text{C}_{18}\text{H}_{16}\text{N}_2\text{O}_3$  (658.09) (%): Calc: C 32.85, N 4.26, H 2.45; found: C 32.49, N 4.07, H 2.19.

IR (KBr pellets,  $\nu \text{ cm}^{-1}$ ): 3462 (s), 3055 (m), 2964 (m), 2930 (w), 2867 (w), 2013 (s), 1966 (s), 1918 (s), 1843 (s), 1662 (m), 1593 (m), 1457 (m), 1445 (m), 1336 (m), 1319 (m), 1282 (w), 1255 (m), 1157 (m), 1088 (w), 1058 (w), 994 (w), 939 (m), 791 (w), 749 (s), 696 (s), 649 (s).

$^1\text{H}$  NMR (400.13 MHz,  $(\text{CD}_3)_2\text{CO}$ , room temp., ppm): 1.05 (t, 3H,  $\text{H}_1$ ), 1.90 (t, 2H,  $\text{H}_2$ ), 3.27 (m, 2H,  $\text{H}_3$ ), 7.30 (dd, 2H,  $\text{H}_{12}$   $\text{H}_{14}$ ), 7.55 (m, 2H,  $\text{H}_{11}$   $\text{H}_{15}$ ), 7.64 (m, 1H,  $\text{H}_8$ ), 7.68 (m, 1H,  $\text{H}_{13}$ ), 8.09 (t, 1H,  $\text{H}_6$ ), 8.16 (d, 1H,  $\text{H}_7$ ), 8.78 (d, 1H,  $\text{H}_9$ ).

$^{13}\text{C}\{^1\text{H}\}$  NMR (400.13 MHz,  $(\text{CD}_3)_2\text{CO}$ , room temp., ppm): 10.5 (C1), 20.5 (C2), 41.9 (C3), 124.3 (C12), 126.5 (C14), 128.0 (C11 C15), 129.7 (C8), 130.7 (C13), 137.6 (C7), 142.3 (C6), 148.3 (C9).

#### 4.4. Synthesis of materials **MCM-WBrL<sub>1</sub>**, **MCM-WIL<sub>1</sub>**, **MCM-WBrL<sub>2</sub>**, **MCM-WIL<sub>2</sub>**, **MCM-MoBrL<sub>2</sub>**, and **MCM-MoIL<sub>2</sub>**

A solution of each complex (0.65 mmol) in dry toluene (10 mL) was added to a suspension of 1 g of the material **MCM-L<sub>1</sub>Si** or **MCM-L<sub>2</sub>Si** in dry toluene (20 mL). The reaction mixture was stirred under a  $\text{N}_2$  atmosphere at room temperature. The resulting material was then filtered off, washed with dichloromethane, and dried under vacuum for 12 h.

**4.4.1.  $\text{MCM}[\text{WBr}_2(\text{CO})_3\text{C}_5\text{H}_4\text{NCH} = \text{N}(\text{CH}_2)_2\text{CH}_3]$  (**MCM-WBrL<sub>1</sub>**, pink powder)**

Elemental analysis (%) found C 10.57, N 2.39, H 1.95, W 4.44.

IR (KBr  $\nu \text{ cm}^{-1}$ ) 2981 (m), 2952 (w), 2893 (w), 2044, 1931, 1853 (m;  $\nu_{\text{C}=\text{O}}$ ), 1624 (s;  $\nu_{\text{C}=\text{N}}$ ), 1475 (w), 1460 (w), 1390 (m), 1244 (vs), 1087 (vs), 968 (vs), 795 (s).

$^{13}\text{C}$  CP MAS NMR ( $\delta$  ppm) 9.22 ( $\text{SiCH}_2$ ), 17.30 ( $\text{SiOCH}_2\text{CH}_3$ ), 21.06 ( $\text{CH}_2\text{CH}_2\text{CH}_2$ ), 42.76 ( $\text{CH}_2\text{N}$ ), 58.21 ( $\text{SiOCH}_2\text{CH}_3$ ).

$^{29}\text{Si}$  MAS NMR ( $\delta$  ppm) -49.49 ( $\text{T}^1$ ), -57.76 ( $\text{T}^2$ ), -67.78 ( $\text{T}^3$ ), -104.39 ( $\text{Q}^3$ ), -109.93 ( $\text{Q}^4$ ).

**4.4.2.  $\text{MCM}[\text{WI}_2(\text{CO})_3\text{C}_5\text{H}_4\text{NCH} = \text{N}(\text{CH}_2)_2\text{CH}_3]$  (**MCM-WIL<sub>1</sub>**, pink powder)**

Elemental analysis (%) found C 9.86, N 2.16, H 1.78, W 3.3.

IR (KBr  $\nu \text{ cm}^{-1}$ ) 2976 (w), 2920 (w), 2033, 1944, (m;  $\nu_{\text{C}=\text{O}}$ ), 1622 (s;  $\nu_{\text{C}=\text{N}}$ ), 1448 (w), 1392 (w), 1227 (vs), 1066 (vs), 949 (vs), 789 (s).

$^{13}\text{C}$  CP MAS NMR ( $\delta$  ppm) 9.06 ( $\text{SiCH}_2$ ), 16.79 ( $\text{SiOCH}_2\text{CH}_3$ ), 20.91 ( $\text{CH}_2\text{CH}_2\text{CH}_2$ ), 42.88 ( $\text{CH}_2\text{N}$ ), 58.12 ( $\text{SiOCH}_2\text{CH}_3$ ).

$^{29}\text{Si}$  MAS NMR ( $\delta$  ppm) -48.72 ( $\text{T}^1$ ), -58.79 ( $\text{T}^2$ ), -67.45 ( $\text{T}^3$ ), -101.61 ( $\text{Q}^3$ ), -110.66 ( $\text{Q}^4$ ).



#### 4.4.3. **MCM-[WBr<sub>2</sub>(CO)<sub>3</sub>C<sub>5</sub>H<sub>4</sub>NCCH<sub>3</sub> = N(CH<sub>2</sub>)<sub>2</sub>CH<sub>3</sub>] (MCM-WBrL<sub>2</sub>, orange powder)**

Elemental analysis (%) found C 7.29, N 2.25, H 1.82, W 3.4.

IR (KBr  $\nu$  cm<sup>-1</sup>) 3053 (w), 2968 (m), 2945 (w), 2879 (w), 2015, 1955, 1865 (s;  $\nu_{C=O}$ ), 1632, 1591 (s;  $\nu_{C=N}$ ), 1539 (w), 1491 (w), 1460 (m), 1392 (m), 1230 (vs), 1147 (vs), 1061 (vs), 893 (s), 820 (vs), 582 (s).

<sup>13</sup>C CP MAS NMR ( $\delta$  ppm) 9.8 (SiCH<sub>2</sub>), 17.7 (SiOCH<sub>2</sub>CH<sub>3</sub>), 21.2 (CH<sub>2</sub>CH<sub>2</sub>CH<sub>2</sub>), 42.6 (CH<sub>2</sub>N), 58.3 (SiOCH<sub>2</sub>CH<sub>3</sub>), 59.9 (SiOCH<sub>2</sub>CH<sub>3</sub>), 67.9 (CH<sub>3</sub>-ring), 125.5, 128.9, 137.6, 144.4 (Ph ring), 198.7.

<sup>29</sup>Si MAS NMR ( $\delta$  ppm) -59.0 (T<sup>2</sup>), -67.6 (T<sup>3</sup>), -102.4 (Q<sup>3</sup>), -109.8 (Q<sup>4</sup>).

#### 4.4.4. **MCM-[WI<sub>2</sub>(CO)<sub>3</sub>C<sub>5</sub>H<sub>4</sub>NCCH<sub>3</sub> = N(CH<sub>2</sub>)<sub>2</sub>CH<sub>3</sub>] (MCM-WIL<sub>2</sub>) (orange powder)**

Elemental analysis (%) found C 6.91, N 1.09, H 1.55, W 4.47.

IR (KBr  $\nu$  cm<sup>-1</sup>) 3055 (w), 2987 (m), 2935 (w), 2879 (w), 2023, 1952, 1876 (s;  $\nu_{C=O}$ ), 1707 (m), 1648, 1616 (vs;  $\nu_{C=N}$ ), 1529 (w), 1473 (w), 1458 (w), 1387 (m), 1232 (vs), 1113 (vs), 1063 (vs), 906 (s), 814 (vs), 590 (s).

<sup>13</sup>C CP MAS NMR ( $\delta$  ppm) 9.7 (SiCH<sub>2</sub>), 17.6 (SiOCH<sub>2</sub>CH<sub>3</sub>), 21.0 (CH<sub>2</sub>CH<sub>2</sub>CH<sub>2</sub>), 42.6 (CH<sub>2</sub>N), 58.2 (SiOCH<sub>2</sub>CH<sub>3</sub>), 60.0 (SiOCH<sub>2</sub>CH<sub>3</sub>), 125.3, 129.0, 137.6, 148.7 (Ph ring), 197.8.

<sup>29</sup>Si MAS NMR ( $\delta$  ppm) -58.4 (T<sup>2</sup>), -66.8 (T<sup>3</sup>), -102.2 (Q<sup>3</sup>), -109.4 (Q<sup>4</sup>).

#### 4.4.5. **MCM-[MoBr<sub>2</sub>(CO)<sub>3</sub>C<sub>5</sub>H<sub>4</sub>NCCH<sub>3</sub> = N(CH<sub>2</sub>)<sub>2</sub>CH<sub>3</sub>] (MCM-MoBrL<sub>2</sub>, pink powder)**

Elemental analysis (%) found C 6.83, N 2.16, H 1.91, Mo 5.11.

IR (KBr  $\nu$  cm<sup>-1</sup>) 3033 (w), 2976 (m), 2922 (w), 2883 (w), 2003, 1934, 1853 (s;  $\nu_{C=O}$ ), 1707 (m), 1677, 1610 (s;  $\nu_{C=N}$ ), 1493 (w), 1448 (m), 1396 (m), 1240 (vs), 1117 (vs), 796 (vs), 721 (vs), 582 (s).

<sup>13</sup>C CP MAS NMR ( $\delta$  ppm) 9.0 (SiCH<sub>2</sub>), 18.0 (SiOCH<sub>2</sub>CH<sub>3</sub>), 21.5 (CH<sub>2</sub>CH<sub>2</sub>CH<sub>2</sub>), 25.8 (CH<sub>2</sub>CH<sub>2</sub>CH<sub>2</sub>), 42.9 (CH<sub>2</sub>N), 60.0 (SiOCH<sub>2</sub>CH<sub>3</sub>), 69.2 (CH<sub>3</sub>-ring), 125.8, 129.4 (Ph ring).

<sup>29</sup>Si MAS NMR ( $\delta$  ppm) -58.3 (T<sup>2</sup>), -66.7 (T<sup>3</sup>), -102.1 (Q<sup>3</sup>), -109.6 (Q<sup>4</sup>).

#### 4.4.6. **MCM-[MoI<sub>2</sub>(CO)<sub>3</sub>C<sub>5</sub>H<sub>4</sub>NCCH<sub>3</sub> = N(CH<sub>2</sub>)<sub>2</sub>CH<sub>3</sub>] (MCM-MoIL<sub>2</sub>, pink powder)**

Elemental analysis (%) found C 7.19, N 2.31, H 1.84, Mo 5.97.

IR (KBr  $\nu$  cm<sup>-1</sup>) 3049 (w), 2979 (m), 2937 (w), 2893 (w), 2023, 1946, 1871 (s;  $\nu_{C=O}$ ), 1671, 1606 (s;  $\nu_{C=N}$ ), 1469 (w), 1444 (m), 1387 (m), 1246 (vs), 1142 (vs), 1051 (vs), 914 (s), 810 (s), 579 (s).

<sup>13</sup>C CP MAS NMR ( $\delta$  ppm) 10.0 (SiCH<sub>2</sub>), 17.4 (SiOCH<sub>2</sub>CH<sub>3</sub>), 21.1 (CH<sub>2</sub>CH<sub>2</sub>CH<sub>2</sub>), 25.5 (CH<sub>2</sub>CH<sub>2</sub>CH<sub>2</sub>), 42.9 (CH<sub>2</sub>N), 59.9 (SiOCH<sub>2</sub>CH<sub>3</sub>), 68.0 (CH<sub>3</sub>-ring), 125.6, 128.6, 129.2 (Ph ring).

<sup>29</sup>Si MAS NMR ( $\delta$  ppm) -57.9 (T<sup>2</sup>), -66.7 (T<sup>3</sup>), -102.4 (Q<sup>3</sup>), -109.8 (Q<sup>4</sup>).

#### 4.5. Crystallography

X-ray diffraction data were collected at low temperature with monochromated Mo-K $\alpha$  radiation (MoK $\alpha$  ( $\lambda$  = 0.71073 Å) on a Bruker Kappa APEX II diffractometer equipped with a CCD area detector. Absorption corrections were applied using SADABS [46]. The structures were solved by intrinsic phasing with SHELXT [47] and refined by least-squares methods with SHELXL [48], using the Olex2 software [49]. All non-hydrogen atoms were refined with anisotropic thermal parameters. The hydrogen atoms were positioned in geometrically idealized positions and refined using the riding model. All molecular diagrams were made with Mercury [50].

The Crystal data and selected refinement details are listed in Table S4. The structures were deposited with the Cambridge Crystallographic Data Centre with the numbers 1,975,301 (WBrL<sub>1</sub>) and 1,975,301 (WIL<sub>1</sub>).

#### 4.6. Computational studies

Density Functional Theory calculations [38] were carried out using the Amsterdam Density Functional program (ADF) [39–41]. Geometries were optimized with gradient correction, without symmetry constraints, using the Local Density Approximation of the correlation energy (Vosko-Wilk-Nusair) [51] and the Generalized Gradient Approximation (Becke's [52] exchange and Perdew's [53,54] correlation functionals). The COSMO approach implemented in ADF was considered to take into account solvent (dichloromethane) in all geometry optimizations and single point calculations. Relativistic effects were treated with the ZORA approximation [55]. Triple  $\zeta$  Slater-type orbitals (STO) with a small frozen core were used to describe all the valence electrons of H, O, C, N, Br, I, Mo and W. A set of two polarization functions was added to all atoms. Frequency calculations were carried out to check that intermediates were minima in the potential energy surface. Three-dimensional representations of the structures and molecular orbitals were obtained with Chemcraft [56].

The geometries were modelled from the structures described above and from that of [Mo( $\eta^3$ -C<sub>3</sub>H<sub>5</sub>)Br(CO)<sub>2</sub>(L<sub>1</sub>)]. In the search for the intermediates, several isomers of A and B were tested. For the B type species, B and B' described above have close energies and can be interconverted. Although B was the more stable, it could not be found for the iodide complexes.

#### Declaration of Competing Interest

The authors declare that they have no known competing financial interests or personal relationships that could have appeared to influence the work reported in this paper.

#### Acknowledgements

We thank the Fundação para a Ciência e a Tecnologia (FCT), Portugal, for financial support to Centro de Química e Bioquímica (UID/MULTI/00612/2019), Centro de Química Estrutural (UIDB/00100/2020 and UIDP/00100/2020), and BioISI – Biosystems & Integrative Sciences Institute UIDB/04046/2020 and UIDP/04046/2020). M. Vasconcellos-Dias thanks FCT for a PhD grant (SFRH/BD/37690/2007). The crystallographic studies were supported by CICECO-Aveiro Institute of Materials (UIDB/50011/2020 & UIDP/50011/2020), financed by National Funds through the FCT/MEC, and co-financed by QREN-FEDER through COMPETE under the PT2020 Partnership Agreement. We acknowledge M. S. Saraiva and P. Ferreira for help with some catalytic reactions and solid-state NMR, respectively.

#### Appendix A. Supplementary data

Supplementary data to this article can be found online at <https://doi.org/10.1016/j.ica.2021.120263>.

#### References

- [1] S.S. Balula, S.M. Bruno, A.C. Gomes, A.A. Valente, M. Pillinger, I.S. Gonçalves, D.J. Macquarrie, J.H. Clark, *Inorg. Chim. Acta* 387 (2012) 234–239.
- [2] A. Mentes, M.E. Hanhan, *Transition Met. Chem.* 33 (2008) 91–97.
- [3] S.R. Gilani, Z. Mahmood, *J. Chem. Soc. Pak.* 25 (2003) 41–43.
- [4] A.C. Gomes, S.M. Bruno, S. Gago, R.P. Lopes, D.A. Machado, A.P. Carminatti, A. Valente, M. Pillinger, I.S. Gonçalves, *J. Organomet. Chem.* 696 (2011) 3543–3550.
- [5] A. Mentes, R.D.W. Kemmitt, J. Fawcett, D.R. Russell, *J. Organomet. Chem.* 660 (2002) 91–97.
- [6] A. Mentes, *Transition Met. Chem.* 24 (1999) 77–80.
- [7] G.-E. Matsubayashi, T. Ohara, T. Tanaka, *Inorg. Chim. Acta* 161 (1989) 67–72.
- [8] D.M. Haddleton, D.J. Duncalf, D. Kukulj, M.C. Crossman, S.G. Jackson, S.A.F. Bon, A.J. Clark, A.J. Shooter, *Eur. J. Inorg. Chem.* (1998) 1799–1806.
- [9] S. Shabbir, S. Lee, M. Lim, H. Lee, H. Ko, Y. Lee, H. Rhee, *J. Organomet. Chem.* 846 (2017) 296–304.
- [10] H. Kotze, S. Mapolie, *Appl. Organomet. Chem.* 31 (2016) 1–13.



- [11] F. Hartl, M.J. Bakker, V.F. Santos, P.J. Costa, M.J. Calhorda, *Inorg. Chem.* 57 (2018) 11704–11716.
- [12] M. Vasconcellos-Dias, J. Marreiros, R. Sales, V. Félix, P. Brandão, C.D. Nunes, M. J. Calhorda, *Molecules* 24 (2019) 578.
- [13] M. Vasconcellos-Dias, C.D. Nunes, P.D. Vaz, P. Ferreira, P. Brandão, V. Félix, M. J. Calhorda, *J. Catal.* 256 (2008) 301–311.
- [14] M. Abrantes, A.M. Santos, J. Mink, F.E. Kühn, C.C. Romão, *Organometallics* 22 (2003) 2112–2118.
- [15] J.C. Alonso, P. Neves, M.J. Pires da Silva, S. Quintal, P.D. Vaz, C. Silva, A. A. Valente, P. Ferreira, M.J. Calhorda, V. Félix, M.G.B. Drew, *Organometallics* 26 (2007) 5548–5556.
- [16] M. Vasconcellos-Dias, M.S. Saraiva, P. Ferreira, M.J. Calhorda, *Organometallics* 34 (2015) 1465–1478.
- [17] M. Vasconcellos-Dias, C.D. Nunes, P.D. Vaz, P. Ferreira, M.J. Calhorda, *Eur. J. Inorg. Chem.* (2007) 2917–2925.
- [18] C.D. Nunes, A.A. Valente, M. Pillinger, A.C. Fernandes, C.C. Romão, J. Rocha, I. S. Gonçalves, *J. Mat. Chem.* 12 (2002) 1735–1742.
- [19] B. Marler, U. Oberhagemann, S. Voltmann, H. Gies, *Micropor. Mesopor. Mat.* 6 (1996) 375–383.
- [20] W. Hammond, E. Prouzet, S.D. Mahanti, T.J. Pinnavia, *Micropor. Mesopor. Mat.* 27 (1999) 19–25.
- [21] M.D. Alba, A. Becerro, J. Klinowski, *J. Chem. Soc., Faraday Trans.* 92 (1996) 849–854.
- [22] A.A. Romero, M.D. Alba, W. Zhou, J. Klinowski, *J. Phys. Chem. B* 101 (1997) 5294–5300.
- [23] M. Kruk, M. Jaroniec, *Langmuir* 15 (1999) 5410–5413.
- [24] A. Jimtaisong, R.L. Luck, *Inorg. Chem.* 45 (2006) 10391–10402.
- [25] M.S. Saraiva, C.I. Fernandes, T.G. Nunes, M.J. Calhorda, C.D. Nunes, *Appl. Catal. A* 504 (2015) 328–337.
- [26] M.S. Saraiva, C.I. Fernandes, T.G. Nunes, C.D. Nunes, M.J. Calhorda, *Top. Catal.* 59 (2016) 1237–1248.
- [27] M.S. Saraiva, C.I. Fernandes, T.G. Nunes, C.D. Nunes, M.J. Calhorda, *J. Organomet. Chem.* 751 (2014) 443–452.
- [28] A.A. Valente, J.D. Seixas, I.S. Gonçalves, M. Abrantes, M. Pillinger, C.C. Romão, *Catal. Lett.* 101 (2005) 127–130.
- [29] M. Pratt, J.B. Harper, S.B. Colbran, *Dalton Trans.* (2007) 2746–2748.
- [30] P.J. Costa, M.J. Calhorda, F.E. Kühn, *Organometallics* 29 (2010) 303–311.
- [31] A.M. Al-Ajlouni, D. Veljanovski, A. Capapé, J. Zhao, E. Herdtweck, M.J. Calhorda, F.E. Kühn, *Organometallics* 28 (2009) 639–645.
- [32] F.E. Kühn, M. Groarke, E. Bencze, E. Herdtweck, A. Prazeres, A.M. Santos, M. J. Calhorda, C.C. Romão, I.S. Gonçalves, A.D. Lopes, M. Pillinger, *Chem. Eur. J.* 8 (2002) 2370–2383.
- [33] L.F. Veiros, A. Prazeres, P.J. Costa, C.C. Romão, F.E. Kühn, M.J. Calhorda, *Dalton Trans.* (2006) 1383–1389.
- [34] A. Comas-Vives, A. Lledós, R. Poli, *Chem. Eur. J.* 16 (2010) 2147–2158.
- [35] M.J. Calhorda, P.J. Costa, *Curr. Org. Chem.* 16 (2012) 65–72.
- [36] C.D. Nunes, M.J. Calhorda, *Inorg. Chim. Acta* 431 (2015) 122–131.
- [37] A.C. Gomes, J.A. Fernandes, C.A. Gamelas, I.S. Gonçalves, F.A.A. Paz, *Acta Crystallogr., Sect. E* 67 (2011), m1738.
- [38] R.G. Parr, W. Yang, *Density-Functional Theory of Atoms and Molecules*, Oxford University Press, 1989.
- [39] G. te Velde, F.M. Bickelhaupt, E.J. Baerends, C. Fonseca Guerra, S.J.A. van Gisbergen, J.G. Snijders, T. Ziegler, *Chemistry with ADF. J. Comput. Chem.* 22 (2001) 931–967.
- [40] C. Fonseca Guerra, J.G. Snijders, G. te Velde, E.J. Baerends, *Towards an Order-N DFT Method, Theor. Chem. Acc.* 99 (1998) 391–403.
- [41] Theoretical Chemistry, Vrije Universiteit, Amsterdam, T. N. ADF2013 SCM <http://www.scm.com> (accessed September, 2020).
- [42] P.K. Baker, S.G. Fraser, E.M. Keys, *J. Organomet. Chem.* 309 (1986) 319–321.
- [43] R.G. Hayter, *Synthesis* 13 (1968) 4–6.
- [44] J.M. Maher, N.J. Cooper, *J. Am. Chem. Soc.* 192 (1980) 7606–7607.
- [45] M.S. Saraiva, N.L. Dias Filho, C.D. Nunes, P.D. Vaz, T.G. Nunes, M.J. Calhorda, *Micropor. Mesopor. Mat.* 117 (2009) 670–677.
- [46] L. Krause, R. Herbst-Irmer, G.M. Sheldrick, D. Stalke, *J. Appl. Crystallogr.* 48 (2015) 3–10.
- [47] G.M. Sheldrick, *Acta Cryst., A* 71 (2015) 3–8.
- [48] G.M. Sheldrick, *Acta Cryst., C* 71 (2015) 3–8.
- [49] L.J. Bourhis, O.V. Dolomanov, R.J. Gildea, J.A.K. Howard, H. Puschmann, *Acta Cryst., A* 71 (2015) 59–75.
- [50] C.F. Macrae, I.J. Bruno, J.A. Chisholm, P.R. Edgington, P. McCabe, E. Pidcock, L. Rodriguez-Monge, R. Taylor, J. van de Streek, P.A. Wood, *J. Appl. Crystallogr.* 41 (2008) 466–470.
- [51] S.H. Vosko, L. Wilk, M. Nusair, *Can. J. Phys.* 58 (1980) 1200–1211.
- [52] A.D. Becke, *J. Chem. Phys.* 109 (1998) 2092–2098.
- [53] J.P. Perdew, *Phys. Rev. B* 33 (1986) 8822–8824.
- [54] J.P. Perdew, *Phys. Rev. B* 34 (1986) 7406–7406.
- [55] E. van Lenthe, A. Ehlers, E.-J. Baerends, *J. Chem. Phys.* 110 (1999) 8943–8953.
- [56] Chemcraft Program <http://www.chemcraftprog.com/index.html> (accessed September, 2020).